UNIVERSIDADE BEIRA INTERIOR

Development, implementation, and validation of a condition monitoring platform for vibration analysis on three-phase induction motors

Fábio Alexandre Silva Teixeira de Brito

Dissertação para obtenção do Grau de Mestre em

Engenharia Eletrotécnica e de Computadores

(2º ciclo de estudos)

Orientador: Doutor Fernando José Figueiredo Bento

Setembro de 2024

Declaração de Integridade

Eu, Fábio Alexandre Silva Teixeira de Brito, que abaixo assino, estudante com o número de inscrição M12328 de Engenharia Eletrotécnica e de Computadores da Faculdade de Engenharia, declaro ter desenvolvido o presente trabalho e elaborado o presente texto em total consonância com o **Código de Integridades da Universidade da Beira Interior**.

Mais concretamente afirmo não ter incorrido em qualquer das variedades de Fraude Académica, e que aqui declaro conhecer, que em particular atendi à exigida referenciação de frases, extratos, imagens e outras formas de trabalho intelectual, e assumindo assim na íntegra as responsabilidades da autoria.

Universidade da Beira Interior, Covilhã 16 /09 /2024

(assinatura conforme Cartão de Cidadão ou preferencialmente
assinatura digital no documento original se naquele mesmo formato)

Acknowledgments

This work is the result of the efforts of many people who have surrounded me in recent years, people who believed in me and push me up when I was down. To those who stayed with me, I would like to thank.

Firstly, I want to dedicate this work to my children Mariana and Miguel. I hope that one day, they will look at the example I left them and be inspired. Always believe in your abilities. I want to thank my parents and my sister for the support given during this long journey. I would like to show my deep gratitude to Sandra Antunes, for her intense support in recent years, and for always believing in my abilities. Without Sandra Antunes, I would not have returned to the path of personal development.

I would like to thank all my professors, who taught me the fundamentals that led to the completion of this work. I also wanted to thanks to my university colleagues, with a special thanks to Philipe Cavalcanti Bandeira for all the experiences shared along the past years.

I would like to demonstrate my deep gratitude to my advisor, Dr. Fernando José Figueiredo Bento, for the supervision and for providing me the assistance that allowed me to successfully accomplish this work. I also wanted to leave a consideration word to all members of CISE – Electromechatronic System Research Centre, for providing the technical resources needed for the experimental validation of this work and to Eng. João Craveiro for the suggested theme, as well as the priceless opportunity and support provided.

Resumo

Graças à sua reconhecida robustez e fiabilidade, o motor de indução trifásico afigura-se enquanto máquina elétrica de excelência na grande maioria da indústria. Este dispositivo ocupa um lugar preponderante nas cadeias de produção e em processos auxiliares, assegurando a conversão eletromecânica de energia. Ao mesmo tempo, este dispositivo encontra-se muitas vezes exposto a condições de funcionamento bastante adversas, sendo por isso de especial importância a monitorização contínua da sua condição, com o objetivo de otimizar o tempo de funcionamento e antecipar avarias, diminuindo as perdas financeiras que daí advêm.

O objetivo principal desta dissertação consiste em desenvolver uma plataforma autónoma para a monitorização e o diagnóstico de avarias em motores de indução trifásicos. Nesse sentido, e tendo em conta que a acessibilidade aos equipamentos é, muitas vezes, um fator determinante, como é o caso dos ventiladores em condutas, indústrias com ambientes perigosos ou bombas submersíveis, propõe-se dimensionar, desenvolver, implementar e validar um sistema de aquisição e processamento de sinais analógicos, provenientes de acelerómetros piezoelétricos acoplados à carcaça de um motor de indução trifásico. A informação recolhida pela solução proposta permite informar os utilizadores acerca da condição de funcionamento dos equipamentos, facilitando assim processos de tomada de decisão.

Palavras-chave

Motor de indução trifásico; Diagnóstico de avarias; Sistema de aquisição de sinal; Placa de circuitos impressos; Monitorização de condição; Análise de vibrações.

Abstract

Thanks to its renowned robustness and reliability, the three-phase induction motor is the electrical machine of choice in the vast majority of industries. This device occupies a prominent position in production chains and auxiliary processes. At the same time, this device is often exposed to very adverse operating conditions, which is why continuous monitoring of its condition is particularly important, with the aim of optimising operation and anticipating breakdowns, ultimately reducing the financial losses that eventual faults entail.

The main goal of this dissertation is to develop a platform for monitoring and diagnosing faults in three-phase induction motors. In this sense and considering that accessibility to equipment is often a key factor, as is the case of fans in ducts, industries with hazardous environments or submersible pumps, it is proposed to design, develop, implement, and validate a system for acquiring and processing analogue signals from piezoelectric accelerometers attached to the housing of a three-phase induction motor. The information collected by the proposed solution will enable end users to be informed about the equipment's operating condition, thus facilitating decision-making processes.

Keywords

Three-phase induction motor; Fault diagnosis; Signal acquisition system; Printed circuit board; Condition monitoring; Vibration analysis.

Index

Chapter 1 1
Introduction 1
1.1. Background 1
1.2. Motivation 3
1.3. Objectives 4
1.4. Overview and Organization of the Dissertation 4
1.5. State of the Art 5
1.5.1. Induction Motors and Bearings 6
1.5.2. Data Acquisition System 9
1.5.3. Vibration analysis 11
1.5.4. Fourier Analysis 14
Chapter 2 15
Characterization and sizing of the signal acquisition system 15
2.1. Introduction 15
2.2. Hardware description 16
2.2.1. Electrical and Mechanical Interfaces and Platform Enclosure 18
2.2.2. Microcontroller Functionalities 19
2.2.3. Sensor compatibility and Fast Fourier Analysis (FFT) 19
2.2.4. Conversion between displacement, velocity, and acceleration 21
2.2.5. Data storage, sharing and communication 22
2.2.6. Computing platform selection 22
Chapter 3 25
Signal conditioning circuits 25
3.1. Signal conditioning circuit design 25
Chapter 4 31
Experimental results 31
4.1. Experimental setup and equipment 31
4.2. Motor test with healthy bearing 32
4.3. Motor testing with damaged bearing 41
4.4. Analysis of results 51
Chapter 5 59
Conclusions 59
5.1. General considerations 59
5.2. Suggestions for future work 60

Bibliographic references 61
Appendix 63
PCB Design 63

List of Figures

Figure 1 - Bathtub curve. 2
Figure 2 - Motor reliability study for large motors above 200 HP. 6
Figure 3 - Classification of faults in an induction motor. 7
Figure 4 - Fixed ball bearing: constituent elements and dimensions. 8
Figure 5 – Measurement chain in an automatic control system. 10
Figure 6 - Representation of a sinusoidal signal. 11
Figure 7 - Vibration amplitude as a function of the frequency. 13
Figure 8 - Characterization of parameters in a sinusoidal signal. 13
Figure 9 – Diagram of the electrical circuit 16
Figure 10 - Block diagram for a FFT (Fast Fourier Transform) analyser 20
Figure 11 - Simulation of the second-order low-pass Chebyshev filter in MULTISIM. 26
Figure 12 - Bode diagram of the designed low pass filter. 27
Figure 13 - Schematic diagram of the amplification stage. 28
Figure 14 - Accelerometer signal conditioning circuit. 29
Figure 15 - Visualisation of the signal before the offset gain stage (orange) and after amplification (red). 29
Figure 16 - Laboratory setup for testing the accelerometer signal conditioning system. 32
Figure 17 – Output signal of the vertical axis accelerometer, without load torque. 32
Figure 18 - Signal spectrum of the vertical axis accelerometer output, without load torque. 33
Figure 19 – Output signal of the horizontal axis accelerometer, without load torque. 33
Figure 20 - Signal spectrum of the horizontal axis accelerometer output, without load torque. 34
Figure 21 – Output signal of the axial axis accelerometer, without load torque. 34
Figure 22 – Signal spectrum of the axial axis accelerometer output, without load torque. 35
Figure 23 - Output signal of the vertical axis accelerometer, under half load torque condition. 35
Figure 24 - Signal spectrum of the vertical axis accelerometer output, at half load. 36
Figure 25 – Output signal of the horizontal axis accelerometer, at half load. 36
Figure 26 - Signal spectrum of the horizontal axis accelerometer output, at half load. 37
Figure 27 - Output signal of the axial axis accelerometer, at half load. 37
Figure 28 - Signal spectrum of the axial axis accelerometer output, at half load. 38
Figure 29 – Output signal of the vertical axis accelerometer, at full load torque. 38
Figure 30 - Signal spectrum of the vertical axis accelerometer output, at full load. 39

Figure 31 - Output signal of the horizontal axis accelerometer, at full load. 39
Figure 32 - Signal spectrum of the horizontal axis accelerometer output, at full load. 40
Figure 33 - Output signal of the axial axis accelerometer, at full load. 40
Figure 34 - Signal spectrum of the axial axis accelerometer output, at full load. 41
Figure 35 - Output signal of the vertical axis accelerometer, without load torque and damaged bearing on the outer race. 42
Figure 36 - Signal spectrum of the vertical axis accelerometer output, without load and damaged bearing on the outer race. 42
Figure 37 – Output signal of the horizontal axis accelerometer, without load torque and damaged bearing on the outer race. 43
Figure 38 - Signal spectrum of the horizontal axis accelerometer output, without load and damaged bearing on the outer race. 43
Figure 39 - Output signal of the axial axis accelerometer, without load and damaged bearing on the outer race. 44
Figure 40 - Signal spectrum of the axial axis accelerometer output, without load and damaged bearing on the outer race. 44
Figure 41 - Output signal of the vertical axis accelerometer, at half load condition and damaged bearing on the outer race. 45
Figure 42 - Signal spectrum of the vertical axis accelerometer output, at half load condition and damaged bearing on the outer race. 45
Figure 43 – Output signal of the horizontal axis accelerometer, at half load condition and damaged bearing on the outer race. 46
Figure 44 - Signal spectrum of the horizontal axis accelerometer output, at half load condition and damaged bearing on the outer race. 46
Figure 45 – Output signal of the axial axis accelerometer, at half load condition and damaged bearing on the outer race. 47
Figure 46 - Signal spectrum of the axial axis accelerometer output, at half load condition and damaged bearing on the outer race. 47
Figure 47 – Output signal of the vertical axis accelerometer, at full load condition and damaged bearing on the outer race. 48
Figure 48 - Signal spectrum of the vertical axis accelerometer output, at full load condition and damaged bearing on the outer race. 48
Figure 49 – Output signal of the horizontal axis accelerometer, at full load condition and damaged bearing on the outer race. 49
Figure 50 - Signal spectrum of the horizontal axis accelerometer output, at full load condition and damaged bearing on the outer race. 49

Figure 51 – Output signal of the axial axis accelerometer, at full load condition and damaged bearing on the outer race. 50
Figure 52 - Signal spectrum of the axial axis accelerometer output, at full load condition and damaged bearing on the outer race. 50
Figure 53 - Distribution of measurement points for testing vibration. 51
Figure 54 – Vibration spectrogram obtained for healthy motor condition, in the no-load regime, for the three measurement axes. 53
Figure 55 - Vibration spectrogram obtained for healthy motor condition, in the half load torque regime, for the three measurement axes. 53
Figure 56 - Vibration spectrogram obtained for healthy motor condition, in full load torque regime, for the three measurement axes. 54
Figure 57 – Vibration spectrogram obtained for the faulty bearing, with a 2 mm hole in the outer ring, under no-load condition. 55
Figure 58 - Vibration spectrogram obtained for the faulty bearing, with a 2 mm hole in the outer ring, under half load torque condition. 55
Figure 59 - Vibration spectrogram obtained for the faulty bearing, with a 2 mm hole in the outer ring, under full load torque condition. 56
Figure 60 - Sheet 1 of the electronic circuit schematic. 63
Figure 61 - Sheet 2 of the electronic circuit schematic. 64
Figure 62 - Top layer. 65
Figure 63 - Bottom layer. 65
Figure 64 - Inner 1 layer. 66
Figure 65 - Inner 2 layer. 66

List of Tables

Table 1 - Dynamic performance of the industrial accelerometer EMERSON A0760GP. 17
Table 2 - Electrical interfaces of the ESP32. 18
Table 3 - Platform enclosure specifications. 19
Table 4 - Condition monitoring operating modes. 19
Table 5 - Accelerometer characteristics. 20
Table 6 - FFT performance metrics. 20
Table 7 - Communication protocols for data sharing. 22
Table 8 - Microcontroller characteristics. 23
Table 9 - Dimensions, properties, and performance of the SKF 6206-2Z bearing. 51
Table 10 - Point frequencies on the outer ring for different load torques. 52
Table 11 - Table of characteristic frequencies in different operating regimes. 52
Table 12 - Amplitudes for no-load condition. 57
Table 13 - Amplitudes for half-load condition. 57
Table 14 - Amplitudes for full-load condition. 57

List of Acronyms

FFT	Fast Fourier Transform
RISC-V	Reduced Instruction Set Computing – fifth version
IoT	Internet of Things
RMS	Root Mean Square
IP	Ingress Protection
EMC	Electromagnetic Compatibility
E&E	Electrical & Electronic
PCB	Printed Circuit Board
ATEX	Explosive Atmosphere
OPAMP	Operational Amplifier
LED	Light-Emitting Diode
CPU	Central Processing Unit
GFT	Generalized Fourier Transform
MCU	Microcontroller Units
SBC	Single Board Computers
JFET	Junction Field-Effect Transistor
RPM	Revolutions Per Minute
ADC	Analog-to-Digital Converter

Chapter 1

Introduction

1.1. Background

The current trend in industrial production units consists of the application of the EN 13306:2010 standard, which defines the structuring of a plan for equipment maintenance. This standard rakes into account “safety and any other mandatory requirements associated with the item; consider any impact on the environment and ensure the durability of the item and/or the quality of the product or service provided taking into account costs where necessary.” The person responsible for maintenance is responsible for developing maintenance plans deemed suitable to monitor the evolution of the equipment life cycle and, at the same time, to minimize the factory's production downtime, to meet the established productivity goals.

As the three-phase induction motor is the main component for electromechanical energy conversion in most industries and, concurrently, the responsible for the largest share of electrical energy consumption worldwide, it is natural that induction motors become subject of special attention when it comes to maintenance. A failure in an induction motor potentially leads to the stoppage of production chains. Until the repair or replacement of the faulty motor is carried out, large production stoppage costs are incurred. Such a situation can be avoided through proper maintenance and monitoring of the equipment.

A maintenance plan based on condition monitoring consists of monitoring the critical system parameter over time and checking its condition, whether in terms of wear, noise, vibration, temperature, lubricant leaks, or analysis of motor supply voltages and currents.

The implementation of a condition monitoring system has an easy economic justification and consists of applying several steps with the ultimate objective of avoiding unforeseen stops. The following maintenance philosophy, which will be briefly discussed for contextualization purposes, is called Condition Monitoring Maintenance or Conditioned Maintenance. The first step is to identify which machines and equipment are to be monitored, seeking to answer the following questions: “is the machine critical for production?”, “is the machine critical for quality?”, “does the machine impacts production costs?”, “does the machine implies high maintenance costs?”, “is the machine critical for safety?”, “does the machine have negative effects on the environment?”, “is it economically

viable to monitor the machine?". Having obtained answers to the most pertinent questions, the second step is to define which faults are intended to be diagnosed in each machine. For three-phase induction motors, these malfunctions can take the form of mechanical or electrical imbalance, misalignment, rolling elements degradation, loosening or clearance. The third step consists of choosing the inspection technique to use. Such selection mostly depends on the failure modes to be diagnosed and on the adequacy of the diagnostic approaches to handle such fault types. Inspection techniques commonly considered are thermal analysis, oil analysis, particle detection, iron printing, among others. Taking as a principle that the diagnostic method defined for this dissertation is vibration analysis, possible faults in the three-phase induction motor are identified via vibration analysis. It should be noted that the diagnostic of inter-turn short-circuits faults or broken rotor bars based on vibration analysis is not particularly effective [1]. In condition monitoring based on vibration analysis, the overall level, the shock to the bearings and the frequency spectrum are typically evaluated.

The fourth step consists of the measurement procedures - in this case vibrations. The machine layout is initially evaluated. Upon careful evaluation, the location of the measurement points is defined. Also, it is defined what measurements are taken, what parameters are intended to be measured, how sensors are fixed to the equipment and which equipment is most appropriate for collecting data.

The fifth step consists of processing the information, collected using the inspection technique. In practice, this consists of evaluating the behaviour trend of the three-phase induction motor. This trend is a function of the percentage of failures over the machine lifespan. Typically, this curve, represented in Figure 1, is called a "bathtub curve" [2].

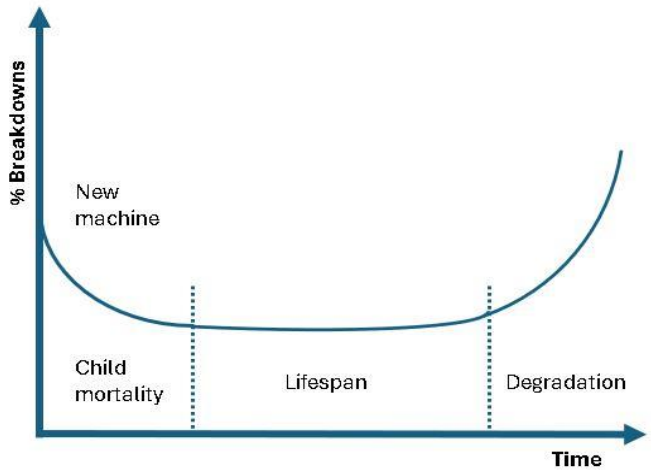

Figure 1 - Bathtub curve.

It is in this step that the diagnosis is made. In other words, fault "signatures" are obtained through an analysis of measured motor parameters. Such analysis can either be performed in the time, frequency, or time-frequency domain. This step consists of evaluating the results obtained from measurements carried out on the equipment. At this stage, it is important to collect a good amount of information to guarantee an excellent quality of results, allowing to detect as many failures as possible, as early as possible, while avoiding dubious diagnostic results, known as "false positive". To minimise the risk of "false positives", the appropriate choice of the diagnostic method is important. When evaluating the results from measurements of vibrations in electrical machines, a simple rule is applied that identifies the existence of a problem when the amplitude of a vibration doubles. If the amplitude of the vibration changes to the triple of the initially verified amplitude, the equipment must be placed for repair, i.e., must be put out of service [2].
As the term itself indicates, condition monitoring maintenance is based on the principle of monitoring the evolution of wear on equipment and its components over time, to obtain a particularly important indicator in this maintenance philosophy, which is the history of the machine. If analysed from a theoretical point of view, the measurement periodicity rule recommends that the interval between different measurements should be defined by the average time between failures. When the reliability of the system to be monitored is at the top of the priority list and is subject of special attention, the frequency of measurements must be higher, with a minimum of six measurements between the average failure time being reasonable. However, several parameters can change the periodicity between measurements, such as the operating regime, the importance of the equipment, its history, the control methodology, the condition of the machine and the availability of qualified labour to carry out the measurements. Once this periodicity has been defined, the next step is to plan the inspections. The essential part of planning is the organization of the routes. The inspection route is made up of a set of equipment that share the inspection periodicity. The definition of route planning consists of preparing a list of machines based on their location, listing the inspection frequency of each machine, identifying the number of measurements on each machine, and calculating the number of measurements per route. That said, machines are typically grouped into routes and the inspection sequence is defined for each route [2].

1.2. Motivation

We currently live in the information age; we have at our fingertips an amount of data that we would hardly have imagined a few decades ago. The three-phase induction motor is a machine capable of providing large amounts of information about its operating status. Having the ability to collect and process all this information remotely to assess the

physical condition of such an important equipment, in real time, represents a significant gain for productivity and for the economy, since electric motors are present in most of the world's industries, from the simplest to the most sophisticated, and are responsible for the largest share of electricity consumption worldwide.

The significant costs related to periodic inspections in industries, the time spent preparing work orders, technical reports and repairs, combined with the limited availability of qualified personnel to monitor and repair these machines, motivate the development of an embedded monitoring system of electrical machines, capable of transmitting data to a central system and facilitating all production and maintenance actions within an organization. That said, the optimization of this task in traditional conditioned maintenance philosophy is of particular importance and motivates the development of this work [3].

1.3. Objectives

The objective of this dissertation is to develop a data acquisition system from piezoelectric accelerometers, coupled to the housing of a three-phase squirrel cage induction motor, in three different axes, namely horizontal, vertical, and axial axis, which performs the conditioning of the respective signals and digitize them using a RISC-V architecture microcontroller. After that, the system computes the Fast Fourier Transform (FFT) and transmits the results via Wi-Fi to a server, allowing a remote analysis of the induction motor condition, thus translating into a valid system that adds value to the industry.

1.4. Overview and Organization of the Dissertation

This dissertation is structured as follows:

Chapter 1: “Introduction” – Signal acquisition platforms are contextualized, namely in the philosophy of condition monitoring maintenance, where this approach is developed in an industrial context. The analysis of the state of the art on signal acquisition systems, vibration analysis using the FFT, three-phase induction motor construction and features, and the diagnostic methods for analysing mechanical vibrations in induction motor bearings is presented.

Chapter 2: “Characterization and sizing of the signal acquisition system” – This chapter describes the stages involved in the design of the signal conditioning circuits and the preparation of the schematic diagram.

Chapter 3: “Printed circuit board creation and testing.” – In this chapter, a description of the characteristics of a signal acquisition system is made. Also, this chapter provides a

presentation of the development stages of the system, the simulation of the various stages in the signal conditioning process and the visualization of the system output.
Chapter 4: “Development of tests on the three-phase induction motor.” – This chapter describes the experimental setup, and the equipment used. Experimental results are provided and a comparison between the different test scenarios is carried out. The effectiveness of the acquisition system tested for both healthy motor conditions and bearing fault conditions is evaluated.
Chapter 5: “Conclusion and suggestions for future work.” – A global assessment of the work carried out is made. The main conclusions are summarised and some suggestions for future work are mentioned.

1.5. State of the Art

Industry 4.0 is currently a widespread reality. Production processes already incorporate several sensors and actuators that communicate among each other and provide supervision with real-time data that assists in the evaluation and monitoring of production, helping to extend the useful life of the expensive equipment integrated in industrial production lines. Huge numbers of devices communicate with each other, a fact that coined the term Internet of Things (IoT). In the current context, the maintenance philosophy based on Condition Monitoring goes hand in hand with the increasingly smaller chips with greater computational power, various software techniques and various communication protocols. Altogether, these components make up sensor networks, which open up new possibilities and advantages [4].
At present, there are several challenges associated with the development of Condition Monitoring maintenance, when comparing it with other maintenance methodologies, such as preventive and reactive maintenance. Costs vary according to the degree of complexity of the system to be monitored. The different operating modes of equipment, as well as the environmental conditions in which they operate and the degree of criticality of their function in the process, also challenge the adoption of condition monitoring. The ever-increasing hardware requirements intrinsic to the increase in the complexity of the devices targeted for monitoring and the need for high-quality data also challenge the widespread adoption of condition monitoring. Another aspect that should not be overlooked is the security of data, since certain processes involve crucial data about production or business aspects. For such cases, the mitigation of information leaks or possible tampering should not be ruled out.
Faced with such challenges, the adoption of the latest technologies to size and design data acquisition systems has important advantages: increasing reliability in the execution of the maintenance plan; optimized security with regards to information communication, as well

as a reduction in latency and increased reliability; reduced costs incurred with infrastructures and their respective maintenance; greater autonomy of monitoring devices thanks to the various energy saving modes that many microcontrollers have [4].

1.5.1. Induction Motors and Bearings

Induction motors are heavily implemented in industry. Their high performance, high reliability, ease of construction and wide availability of power converters are just a few reasons that place this electric machine at the top of preferences to boost industrial productivity and guarantee the process reliability and security of the facilities.

Induction motors, also known as asynchronous motors, have been the subject of study by specialists in reliability and condition monitoring. To promote prompt identification of anomalies, fault diagnostic methods allow the identification of various types of faults and the and quantification of the corresponding degrees of severity. In the case of induction motors, several components of the machine may be affected by faults, from stator inter-turn short-circuits, broken rotor bars, dynamic and static eccentricities and bearing failures, among others [3]. According to a motor reliability study published in IEEE, the most frequent fault in induction motors found in industry is the bearing failure, accounting for around 41 % in large motors above 200 HP, followed by stator failures, which account for around 37 %, and finally failures associated to the rotor, accounting for around 10% [5].

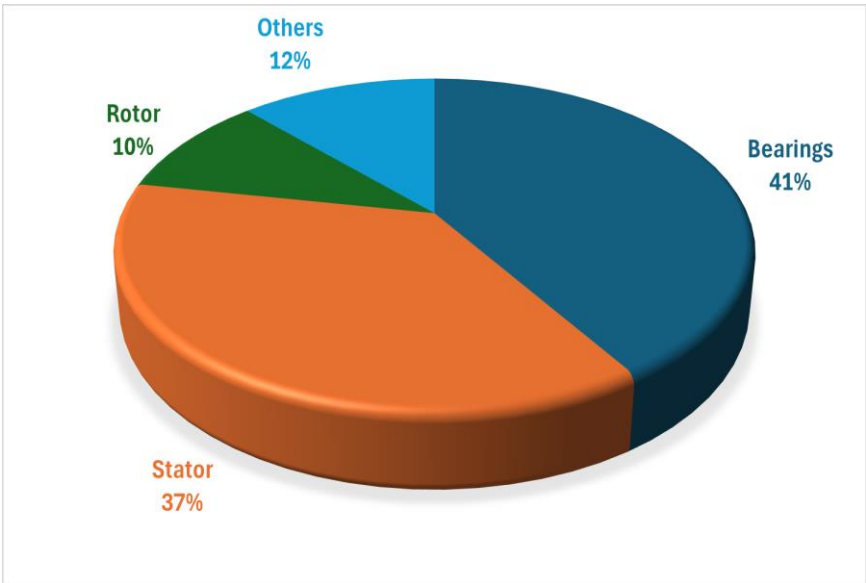

Figure 2 - Motor reliability study for large motors above 200 HP.

The following figure illustrates an overview of the types of faults that may arise in induction motors [3]:

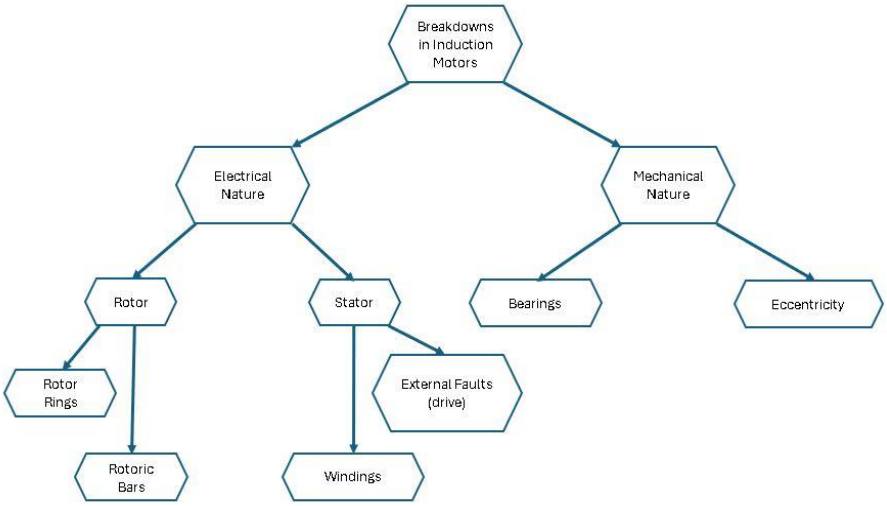

Figure 3 - Classification of faults in an induction motor.

Given the multitude of faults that can arise at three-phase induction motors, it is important to consider fault diagnostic approaches capable of effectively diagnosing most of them. Currently, the most comprehensive diagnostic method consists of analysing the supply currents and voltages with the machine in normal operation. The trend is to evolve towards this technique, which is based on electrical signals. Still, electrical methods are not yet effective for diagnosing bearing faults, which is why the analysis of vibration signals for fault diagnosis is still used [6].

That said, the costs associated to stoppages of large motors easily justify the use of sophisticated maintenance techniques, always with the aim of ensuring continuity of service. Small machines, with low power and dimensions, are also especially important in production lines.

Depending on the root causes, faults in electromechatronic systems may be classified as: 1) evolutionary faults, associated with gradual development; 2) intentional faults, caused deliberately and which interrupt the performance of functions; and 3) catastrophic faults, which lead to the total and immediate stoppage of functions. A catastrophic failure can result in the stoppage of an important drive on the production line and lead to the loss of several hours, or even days, during its repair or replacement. To prevent catastrophic failures from occurring, the first step must consist of analysing the motor power supply quantities, as well as checking the status of the electrical protections, thermal relays, and fuses, thus contradicting the logic of starting the analysis based on the physical state of the motor [3].

A bearing combines distinctive elements in a single device. Its function is to support the movement of a machine's components to minimize, as much as possible, friction in sliding between different parts of the machine. In the case of three-phase induction motor, bearings aim to minimise friction between the bearing and the shaft of the rotor. The bearing is made up of rolling bodies (which can be rollers or spheres), rings with races (either outer or inner ones) and the cage, which consists of the retaining element. Figure 4 illustrates the elements that make up the bearing:

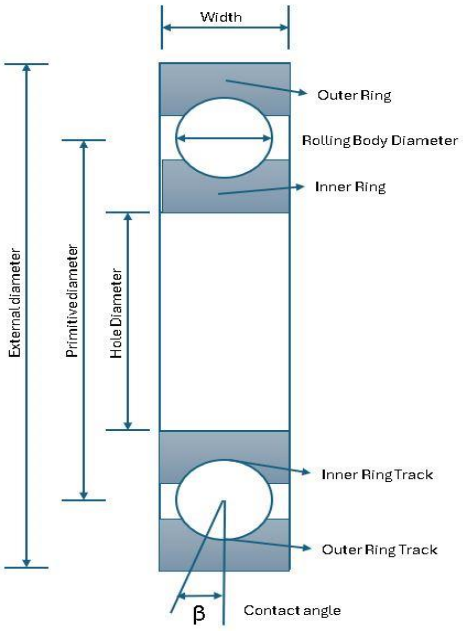

Figure 4 - Fixed ball bearing: constituent elements and dimensions.

Measurements on equipment for collecting vibrometric data begin with a visual inspection. The idea is to identify the best positions for sensing the vibrations around the machine to be analysed, in the components attached to it and in the bearings. The analysis of vibrations arising from damaged bearings can be carried out by attaching an accelerometer as close as possible to the area where the bearing is located. To interpret the acquired data, a comparison is made with reference data, acquired from a healthy motor, so that a conclusion can be drawn. The analysis can be carried out in the temporal domain, in the frequency domain or through probabilistic analyses. Analysis in the frequency domain is the most common approach, using the FFT technique, since it allows to easily identify characteristic frequencies associated with bearing failures. It is possible to assume which of the elements that make up the bearing is damaged, since each element has a specific frequency. To determine the specific frequency arising from vibration, the geometric characteristics of the rolling elements and the mechanical frequency of the rotor are necessary. It is possible to calculate the characteristic frequencies using the following equations [7]:

$$f_{bor} = \frac{N_{cr}}{2} . f_r . \left(1 - \frac{D_{cr}}{D_p} . \cos\beta\right) \quad (1)$$

$$f_{bir} = \frac{N_{cr}}{2} . f_r . \left(1 + \frac{D_{cr}}{D_p} . \cos\beta\right) \quad (2)$$

$$f_{bs} = \frac{D_p}{2D_{cr}} . f_r \left(1 - \left(\frac{D_{cr}}{D_p}\right)^2 . cos^2\,\beta\right) \quad (3)$$

where:

f_{bor} characteristic vibration frequency of the outer race [Hz]

f_{bir} characteristic vibration frequency of the inner race [Hz]

f_{bs} characteristic vibration frequency of the rolling elements [Hz]

f_r rotor mechanical frequency [Hz]

D_p pitch diameter [mm]

D_{cr} rolling body diameter [mm]

N_{cr} number of rolling elements

β contact angle [degrees]

In the instance of a bearing fault, the characteristic fault frequencies are essentially modulated by the electrical supply frequency. In (4), FBNG is the resulting fault frequency component in the stator current, FE is the electrical supply frequency, FV is one of the three characteristic fault frequencies defined by (1) through (3), and m is an integer (m = 1, 2, 3, ...):

$$F_{BNG} = |F_E \pm m * F_V| \quad (4)$$

Since it is widely implemented in maintenance engineering, the analysis of vibrations to detect faults and breakdowns is the subject of a set of technical standards, published by the international Organization for Standardization, namely in the standard ISO 20816 [8]. This standard establishes a relation between the severity of the vibration and the degree of degradation of bearings.

1.5.2. Data Acquisition System

A condition monitoring system based on a signal acquisition system aims to acquire data from electromechanical systems, such as turbomachinery (electric motors coupled to fans,

pumps, or turbines), internal combustion engines or drive systems, and allows an analysis of the condition of the equipment and the evaluation of the status of the various building blocks when detecting known symptoms of developing faults. Signal acquisition systems consist of a chain made up of several blocks for collecting state information, characterized by a certain number of physical and process quantities – see Figure 5.

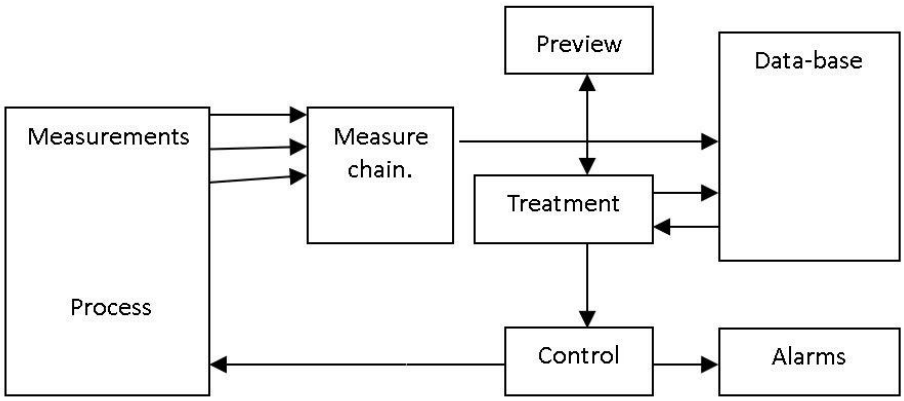

Figure 5 – Measurement chain in an automatic control system.

The first block consists of the measurement process, made up of analogue sensors that capture small physical changes, which can be pressure, temperature, torsion, traction, or compression. Such physical quantities are then converted into electrical signals, which can be voltage, resistance or current. The second block consists of the measurement chain. It is made up of the signal conditioning system, which varies depending on the type of sensor intended to be implemented, the analog-to-digital converter (ADC), responsible for digitizing the signal, and the microprocessor, the component where the information from the sensors is processed and data about the process being monitored is provided. The data from the measurement chain goes to the third block, which is the database. Here, the data is stored and catalogued in order to provide the user with a history of the evolution of the acquired data. The fourth and fifth blocks consist of data processing and visualization, an important aspect in the automatic control system of a process, since the stored data is raw and needs to be interpreted and organized in order to provide information that can be interpreted by the system user. The sixth block consists of the system control algorithm, that depends on the processing of information from the process to be analysed. The control aims to evaluate the system output and, if necessary, make the necessary adjustments so that the system remains operational without the need for external intervention. If it detects an error or a parameter that has previously been stated, the system will have the capacity to resort to the seventh block which consists of triggering alarms, a sign that something in the process is not operational, or certain parameters have

been identified that require more attention or even external intervention in order to safeguard the normal functioning of the process [8].

The information acquired and processed can be accessed either locally or remotely, and the system must have the capacity to transmit information and maintain data for long periods of time, to safeguard any periods of absence of means of communication.

There are several manufacturers of data acquisition systems on the market - most of them international manufacturers - with the capacity to acquire different physical quantities, with a variety of channel numbers and different assemblies. The application of this type of systems covers a wide range of options, ranging from the laboratory to mobile applications, experimental analysis, environmental analysis, and monitoring of industrial processes.

Depending on its applicability and technical sophistication, the indicative price for this type of equipment varies from 70 €, for meteorological systems, to tens of thousands of euros for all-in-one, digital embedded systems with the ability to record data and integrate into more complex systems, typically used in sophisticated industrial facilities [2].

The development of a data acquisition system for Industry 4.0 implies its certification to operate in dangerous locations, often classified as dangerous zones with the possibility of explosions. In these cases, the system to be developed must comply with European directives relating to ATEX certification, directive 94/9/EC, related to the manufacture and sale of Ex equipment, and directive 1999/92/EC, related to the classification of hazardous areas, the correct installation and maintenance of equipment [9]

1.5.3. Vibration analysis

In nature, all bodies vibrate. They do so around a position of equilibrium. The simplest vibration consists of harmonic vibration. Its periodic variation over time can be represented by a sinusoidal function, as depicted in Figure 6.

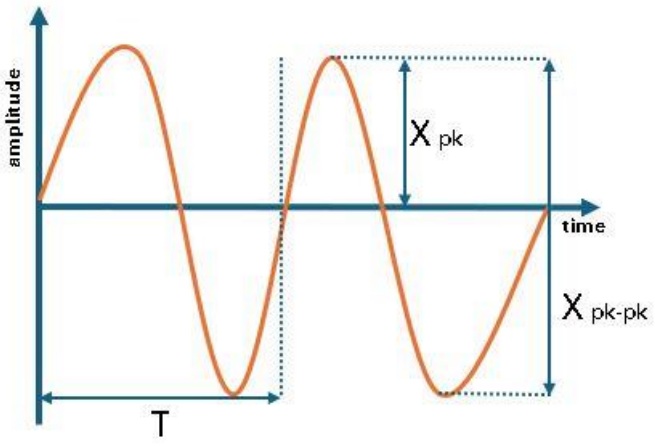

Figure 6 - Representation of a sinusoidal signal.

In this representation, T corresponds to the period and X denotes the amplitude. The period and frequency of a sinusoidal function can be calculated as follows:

$$T = \frac{1}{f} \tag{5}$$

and

$$f = \frac{1}{T} \tag{6}$$

where f represents the frequency, which can be expressed in Hertz or, in the case of rotating machines, revolutions per minute (RPM). Sixty revolutions per minute corresponds to a frequency of 1 Hz.

The vibration amplitude gives an indication of the maximum value that occurs. This parameter does not consider variation over time. The vibration amplitude gives an indication of the maximum value and can be expressed as displacement [mm], the most suitable parameter for low frequencies - typically up to 10 Hz:

$$X = \boldsymbol{x.\sin(\omega t)} \tag{7}$$

Displacement can also be expressed as speed [mm/s], the most suitable parameter for a medium range of frequencies - typically from 10 Hz to 1000 Hz:

$$V = \frac{dx}{dt}\left(\frac{\boldsymbol{dx}}{\boldsymbol{dt}}\right) = \boldsymbol{Wx.\cos(\omega t) = Wx.\sin\left(\omega t + \frac{\pi}{2}\right)} \tag{8}$$

Alternatively, displacement can be expressed as acceleration [G], the most suitable parameter for measurements at high frequencies - typically measurements above 1000 Hz:

$$a = \frac{d}{dt}\left(\frac{\boldsymbol{dx}}{\boldsymbol{dt}}\right) = \boldsymbol{-W^2x.\sin(\omega t) = W^2x.\sin(\omega t + \pi)} \tag{9}$$

Figure 7 illustrates the evolution of the different vibration amplitude units across the entire frequency range.

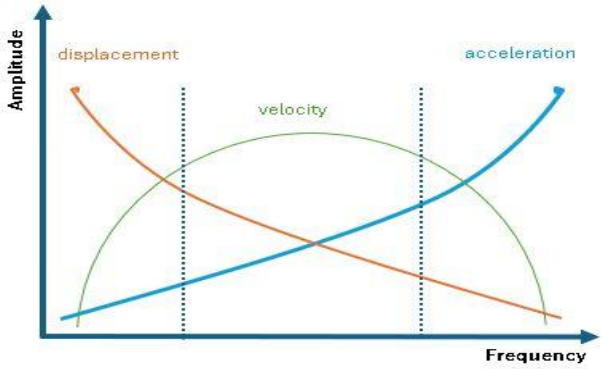

Figure 7 - Vibration amplitude as a function of the frequency.

One of the most common approaches to sense vibration involves the application of piezoelectric accelerometers. For characterizing the signal from piezoelectric accelerometers, it is common to determine its root mean square (RMS). The RMS value of a sinusoidal variable can be obtained using the following equation:

$$X_{rms} = \sqrt{\frac{1}{T}\int_0^T [x(t)]^2 dt} \tag{10}$$

When it is observed for a certain time interval T the RMS value is a quantity that evaluates the energy content associated with the wave signal at the time interval being analysed.
From the point of view of many authors, using the amplitude (peak) or double amplitude (peak to peak) value is the best way to translate the vibratory behaviour of a given piece of equipment, despite the fact that the RMS value is more associated with the energetic content of the vibration, since a signal can have a very high amplitude without having much energy, as long as the duration of this high amplitude is short [10].

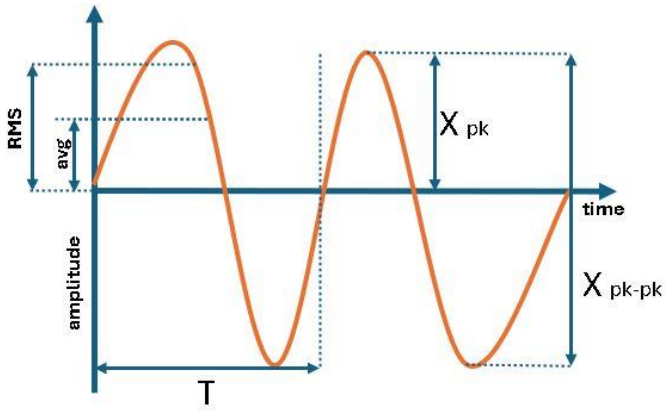

Figure 8 - Characterization of parameters in a sinusoidal signal.

An analysis in the frequency domain consists of changing the representation of the signal in the time domain to a representation in which it is possible to observe which frequencies

are most important in the vibratory phenomenon. It involves replacing a complex signal, which can be periodic or assumed as such, by a sum of simpler harmonic signals and representing the latter based on their amplitude and frequency. From the point of view of vibration analysis, it has the great advantage of allowing each important component of the spectrum to be associated with a specific part of the machine under observation and allowing the study of the frequency components of the signal and their importance [2].

1.5.4. Fourier Analysis

Fourier analysis is of relevant importance in vibration analysis. It allows to express any periodic function as a series of harmonic functions. The Fourier series can be described by the following equation [11]:

$$x(t) = \frac{a_0}{2} + \sum_{n=1}^{\infty} [a_n \cos(n\omega_0 t) + b_n \sin(n\omega_0 t)] \tag{11}$$

where:

$$\omega_0 = \frac{2\pi}{T} \tag{12}$$

is the fundamental frequency and:

$$a_n = \frac{2}{T}\int_t^{t+T} x(t)\cos(n\omega_0 t)dt \tag{13}$$

are the Fourier coefficients, with n = 1, 2, 3, ...

Currently, equipment that performs signal analysis makes use of another signal processing technique based on Fourier analysis, called Fast Fourier Transform, with the English acronym FFT. This operation allows to reduce the number of operations carried out in processing. This algorithm exploits the periodicity and symmetry present in trigonometric functions. The number of algorithm instructions increases; however, the calculation time decreases. In this processing technique, the number of samples in period T must be a power of two. In other words, 256, 512, 1024, 2048, ...samples must be used to compute the FFT, for example.

Chapter 2

Characterization and sizing of the signal acquisition system

The data acquisition platform proposed in this dissertation was designed to acquire vibration signals from electromechanical systems, more specifically from electric motors. Such electric motors may be used to drive different mechanisms, such as turbines, pumps, or fans. The proposed platform facilitates the remote monitoring of electric motors and the real-time assessment of the status of the motor individual components. Particularly, this platform reveals prominent benefits in the evaluation of the condition of bearings installed in induction motors. Operating as a fundamental asset for the end user, the platform design integrates sophisticated technology to meet the rigorous requirements of industry.

2.1. Introduction

This dissertation serves as a reference in the planning and design of a signal acquisition system, outlining the hardware specifications for the platform and emphasizing the essential implementation aspects, so that it can be implemented in an industrial environment. Stipulated hardware requirements cover considerations such as enclosure degree of protection (IP) standards, electromagnetic compatibility (EMC) standards, device operating temperature, power supply requirements, and more. Detailed electrical/electronic (E&E) design specifications include a comprehensive examination of printed circuit board (PCB) layouts, connection protocols, and the chosen microcontroller. The condition monitoring platform for vibration analysis, in three-phase induction motors, provides a versatile and capable industrial embedded system, which aims to achieve two main objectives: 1. Acquire and analyse data from sensors coupled to industrial equipment, in critical processes, to monitor their operation within the scope of the predictive maintenance philosophy; 2. Provide an interface with users in charge of supervising industrial processes.

The design of the system, the choice of components for the system, the analysis of the circuit, up to the optimisation of the printed circuit board (PCB) in electronic design automation (EDA) software, allows full control over all intrinsic aspects of the hardware. ESP32 microcontroller has a solid basis for future iterations and control over the

manufacturing process, allowing parameters and functionalities to be easily changed. Furthermore, it allows changing the format and costs of the signal acquisition board, depending on different project needs.

2.2. Hardware description

The electrical circuit diagram is shown in Figure 9:

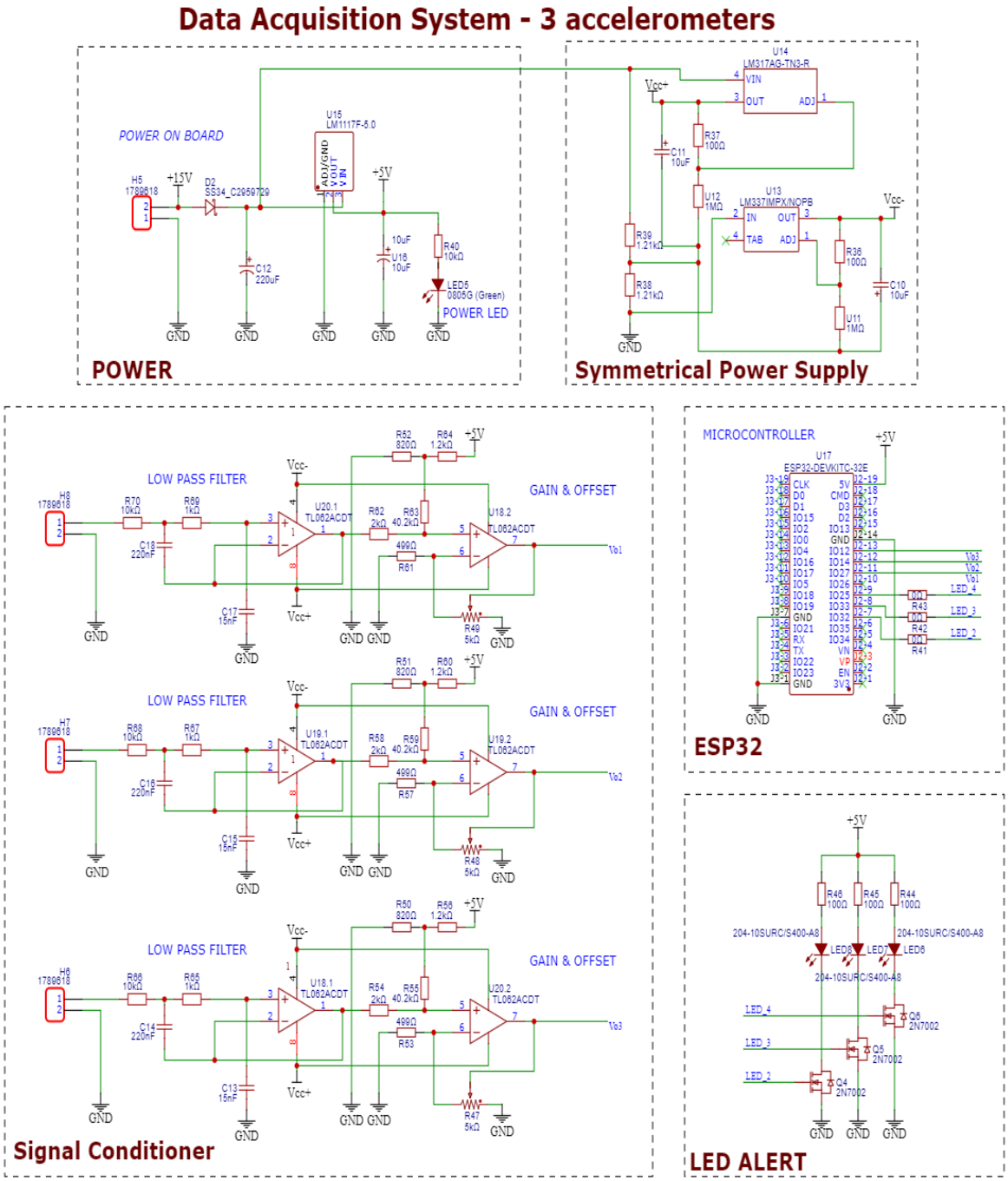

Figure 9 – Diagram of the electrical circuit.

The system, which receives information from three distinctive accelerometers, integrates components for power supply, signal conditioning, processing and status indicators. The data acquisition platform is powered by a 15 V lithium battery, capable of supplying energy to the various components of the system. For components operating at lower voltage, the power supply system also includes a LM1117 voltage regulator, with low voltage drop, which allows a voltage of +5 V to be obtained at its output. The LM1117 voltage regulator is used to power the “Power ON” indicator LED, the signalling LEDs, and the microcontroller. The operational amplifiers (OPAMPs) are powered through two voltage regulators: 1) the LM317, to obtain a positive voltage of +7 V, designated as "*Vcc*+"; and 2) the LM337, to obtain a negative voltage of -7 V, designated as "*Vcc*-". The platform has capacity to connect three piezoelectric accelerometers, which have the dynamic performance characteristics described in Table 1 [12].

Table 1 - Dynamic performance of the industrial accelerometer EMERSON A0760GP.

Dynamic Performance	
Sensitivity (±5 %)	100 mV/g (10.2 mV/m/s²)
Measurement range	±50 g (±490 m/s²)
Frequency range (±3 dB)	0.50 to 10,000 Hz (30 to 600,000 cpm)
Mounted resonant frequency	25 kHz nominal
Amplitude linearity	±1 % (based on straight-line method)
Transverse sensitivity	≤7 %

For vibration monitoring in induction motors, each accelerometer must operate in a frequency range from 0 Hz to 1 kHz. The signal conditioning circuit was designed using a second-order, low-pass Chebyshev filter, integrating TL062ACDT OPAMPs. These OPAMPs feature extremely low power consumption (200 μA), short-circuit protection at the output, low input currents, low polarization, and low offset. To amplify the input signal, the circuit also has adjustable gain capacity, using potentiometers that allow a maximum gain of 100. An additional offset compensation circuit allows the signal to be centred around 1.5 V, since the microcontroller analog inputs must be between 0 V and 3.3 V, a subject that will be discussed with detail further ahead. The platform includes the option of triggering automated alarms or configuring alert levels, using a series of three LEDs that will be used to diagnose various situations, such as imbalances, misalignments, loosening, etc., thus contributing to the protection of systems and processes. Eventually, these events may be integrated into SCADA systems or maintenance management software. The system incorporates a development board with an ESP32-WROOM-32E microcontroller from “Espressif Systems” to process the signals, which are acquired in the time domain, and are processed using an FFT algorithm. The microprocessor will process the signal data acquired in digital form and manipulate it according to the firmware

specifications. The selected microcontroller takes into account the special characteristics in the different functionalities of the microcontroller, such as ADC resolution, communication ports, system clock, different power consumption modes, etc. The microcontroller meets the needs of size, signal processing, energy consumption and cost. The type of microcontroller that will be implemented determines the way in which it will be programmed and the resources available on the integrated circuit. The firmware of the data acquisition system may be based on a finite state machine, that is, an abstract computational model composed of a finite number of states that incorporate information about the current situation of the system. Events are stimuli external to the state machine, which, when triggered, affect the transition to another state. Creating a table where states, events, transitions, and actions are defined could be the starting point for developing the system firmware.

2.2.1. Electrical and Mechanical Interfaces and Platform Enclosure

The platform provides multiple interfaces, through ports on the ESP32 development board. It is important to mention that although there is a wide variety of port types available, it is not expected that all of them will be used simultaneously.

Table 2 characterises the electrical interfaces of the ESP32 development board:

Table 2 - Electrical interfaces of the ESP32.

Interfaces	***Specifications***
Digital I/O	32 channels [0; 3.3] V
Analog I/O	16 inputs to ADC channels
Wi-Fi	2.4 GHz receiver/transmitter (802.11b/g/n)
USB	USB 2.0 (mostly used for development purposes)
Power supply	[0; 5] V, with reverse voltage protection

Of all the interfaces available on the ESP32, three analog inputs will be used to digitize the signal from the accelerometers (ADC2_5; ADC2_6 and ADC2_7) and three GPIO pins will be used to control the transistors associated with the alarm LEDs (GPIO32; GPIO33 and GPIO25), as previously seen in Figure 9.

The objective of this dissertation is to design a platform that will be implemented in industrial environments. Consequently, its shape and casing must meet certain requirements to guarantee its availability and robustness in the face of environmental disturbances. Table 3 contains the specifications necessary to safeguard the functioning of the platform:

Table 3 - Platform enclosure specifications.

Requirements	*Specifications*
EMC	UNECE R10
Ingress Protection (IP)	IP69 [13]
Operating Temperature	[-20, 85] °C
Shock	EN 60068-2-27 [14]
Vibration	EN 60068-2-64 [15]
Dimensions	(L) 85 cm x (W) 90 cm x (H) 5 cm
Connectors	IP69 compatible (e.g. BNC, M12, USB)
ATEX Certification	EN 60079 series [16]

2.2.2. Microcontroller Functionalities

The microcontroller contains two central processing units (CPU) designed to be adaptive and scalable. Each CPU can be controlled individually, and has an adjustable clock frequency, ranging from 80 MHz to 240 MHz This chip has a low power consumption option, allowing to save energy during periods of low utilisation. It integrates generic communication via Wi-Fi, Bluetooth, and Bluetooth Low Energy [17].

The microcontroller processes the acquired signal data, starting by digitising it, and later, in digital form, manipulating the data according to the specifications provided for the firmware. In the microcontroller, condition monitoring involves data acquisition, recording of accelerometer outputs over time, comparison of relevant values with reference ones and recording of significant events. As shown in Table 4, the process of condition monitoring involves operations in the time and frequency domains:

Table 4 - Condition monitoring operating modes.

	Purpose	*Acquisition*	*Processing*	*Records*
Time domain	Acquires the signals from the accelerometers in the time domain	Determines global values – Pk-Pk and RMS	Detects significant events (e.g. increment of the Pk-Pk and RMS values)	Global values – Pk-Pk and RMS
Frequency domain	Determines frequency spectrum of the vibration signal, using a Fourier analysis algorithm (FFT)	Builds frequency spectra (FFT) at regular time intervals, with a maximum frequency range of 1 kHz	Determine the amplitudes of the relevant harmonics	Frequency spectra global value – Pk-Pk and RMS

2.2.3. Sensor compatibility and Fast Fourier Analysis (FFT)

The signal acquisition platform must contain configurable software that allows collecting and analysing data from the accelerometers, according to the specifications described in Table 5.

Table 5 - Accelerometer characteristics.

Specifications	
Industrial accelerometers	Piezoelectric accelerometers (quartz)
Frequency range	0.5 Hz to 1 kHz
Connector arrangement	Top exit, C5015/2 pin
Settling time	≤2 sec (Within 1 % of bias)
Measurement range	± 50 g (±490 m/s²)

For a generic signal represented in the time domain, the microcontroller must provide the possibility of computing the corresponding FFT with the parameters described in Table 6:

Table 6 - FFT performance metrics.

Metric	***Value***
Frequency range	[0,5; 1] kHz
FFT maximum number of points	2048 sample points
FFT maximum computation time	< 100 ms
Sampling frequency	1 kHz

The software must use the function called GFT (Generalized Fourier Transform) to calculate the Fourier transform of a given input signal and return an index of the frequency component with the largest amplitude within the specified frequency range. Figure 10 illustrates the block diagram that illustrates the blocks involved in the FFT analysis. Basically, the input signal is conditioned for better condition monitoring performance and then converted by the ADC (Analog to Digital Converter) from analog to digital signal. Digital data is often called samples.

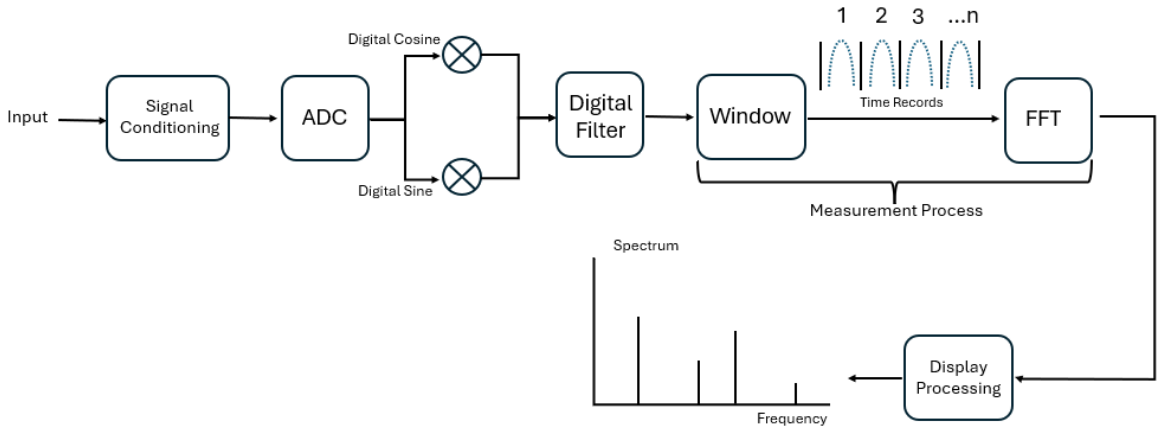

Figure 10 - Block diagram for a FFT (Fast Fourier Transform) analyser.

The function receives two parameters: 1) AUX, which corresponds to an array of floating-point numbers that represent the input signal; and 2) CSF, which represents the cutoff

frequency or sampling rate. A variable, called “timestep” is calculated as the inverse of the sampling rate. The “frequencies” matrix is populated with binary frequency values based on the sampling rate and number of samples. One cycle calculates the Fourier Transform of the input signal by adding the cosine and sine components for each binary frequency value. The Pythagorean theorem is used to calculate the amplitude of each frequency component. Signal sampling by the microcontroller begins with a declaration of local variables to calculate the voltage offset, sampling rate, and time storage in microseconds. That said, the sampling cycle is used to sample the signal several times by reading the analogue value on the corresponding microcontroller pin and storing its values in a matrix, until the defined sampling time is reached. The sampling rate is calculated based on the time spent during the sampling cycle. The sampling frequency must be at least double the highest frequency of the signal. This fundamental rule in the sampling of analog signals is call Nyquist Theorem. For example, a signal containing frequency components up to 1 kHz must be sampled with a sampling rate of at least 2 kHz, to avoid aliasing. Finally, the amplitudes are normalized using the calculation of the voltage displacement value. To normalize these amplitudes, it is necessary to calculate the mean offset of the voltage, denoted by:

$$V_{offset} = \frac{1}{N}\sum_{i=1}^{N} V\ (t_i) \tag{14}$$

where N denotes the total number of samples.
The mean offset of the voltage is then subtracted from the value of the already normalized voltages, thus returning the adjusted voltages.

$$V_{adj}(t) = V_{norm}\ (t) - V_{offset} \tag{15}$$

2.2.4. Conversion between displacement, velocity, and acceleration

When evaluating the data processed on the microcontroller, for a generic signal represented in the frequency domain, the software must be able to convert the units of that same signal, based on operations in the frequency domain. In other words, for a time signal that describes a sinusoidal displacement, it will be possible to carry out its algebraic manipulation with the aim of obtaining its time derivatives. Let us consider the displacement as a sine function:

$$x(t) = A\sin\ (\omega_o t) \tag{16}$$

The speed can be derived from (16) and defined as:

$$v(t) = \omega_o A\cos(\omega_o t) \tag{17}$$

In turn, the acceleration can be derived from (17) and is defined as:

$$a(t) = -\omega_o^2 A\sin(\omega_o t) \tag{18}$$

2.2.5. Data storage, sharing and communication

Data collected from accelerometers is temporarily stored in the memory of the data acquisition platform. The system will have a memory card reader, or alternatively, a flash memory. Since the system is intended to operate in industrial environments, its local memory is valid, but only for short periods. Consequently, the alternative is to share the data collected by the system through the protocols available for ESP32 communication, described in Table 7 [17]. The chosen communication protocol is Wi-Fi, as it allows the ability to export data anywhere, via the internet.

Table 7 - Communication protocols for data sharing.

Communication Interface	***Details***
Wi-Fi	802.11b/g/n
	Bit rate: 802.11n up to 150 Mbps
	A-MPDU and A-MSDU aggregation
	0.4 µs guard interval support
	Centre frequency range of operating channel: 2412 ~ 2484 MHz
Bluetooth	Bluetooth V4.2 BR/EDR and Bluetooth LE specification
	Class-1, class-2 and class-3 transmitter
	AFH
	CVSD and SBC

2.2.6. Computing platform selection

The specifications and requirements for the data acquisition system, described in the previous subsections, provide guidelines for selecting a specific and suitable microcontroller to fulfil the described tasks. The candidates are based on low-power and, simultaneously, low-cost microcontrollers. Among a wide range of options, two possible categories stand out, low-cost Microcontroller Units (MCU) or Single Board Computers (SBC). Given the specifications of the system in question, the option was to use an ESP32 microcontroller from Espressif, with the specifications listed in Table 8 [17].

Table 8 - Microcontroller characteristics.

Category	*Specification*
Processor	32 bits RISC-V MCU - Xtensa® single-/dual-core 32-bit LX6 microprocessor(s)
Memory	448 KB ROM 520 KB SRAM 16 KB SRAM in RTC QSPI supports multiple flash/SRAM chips
Storage	No internal storage
Ethernet	Not available
I/O	34 GPIOs (UART, SPI, SDIO, I2C, LED PWM, Motor PWM, I2S, IR, pulse counter, capacitive touch sensor, 18xADC, 2xDAC)
USB	Used for development
Power supply	5 V
Operating temp	[–40, 85] °C
OS	FreeRTOS

The ESP32 was chosen due to its wide versatility, number of inputs and outputs, and low cost. The disadvantage in relation to an SBC is the difficulty of deploying and writing software in an environment that has more limited hardware resources and is difficult to simulate, which is relevant for carrying out software unit testing.

Chapter 3

Signal conditioning circuits

Signal conditioning is a critical step in the data acquisition chain. The accuracy and reliability of the acquired signals are closely related to the signal conditioning circuit, which needs to measure the signal precisely and effectively. Signal conditioning is necessary to improve the quality of the signal coming from the physical processes, to obtain a better interpretation of the observed phenomena. Each sensor has a different signal conditioning need, so a data acquisition system must always have different signal conditioning circuits to meet the specific needs of the application.

The secret to a well-designed signal conditioning circuit is to understand the principles of operation of the sensor used and the circuitry required to ensure a reliable measurement. The sensors used in instrumentation, whether in industrial, environmental, or structural applications, collect data such as pressure, temperature, flow, or vibrations. To do so, appropriate signal conditioning is needed prior to digitization and processing. There are different signal conditioning techniques such as amplification, attenuation, filtering, isolation, excitation, linearization, cold junction compensation, among others [18].

3.1. Signal conditioning circuit design

The presented platform allows the acquisition of signals from three piezoelectric accelerometers. This type of sensor does not require a power supply and operates according to the piezoelectric effect of a crystal. When subjected to deformation, the crystal generates a difference in the electrical potential. In order to achieve the best possible measurement, it is necessary to understand well the signal conditioning needs that the sensor requires. In this case, the accelerometer needs different types of conditioning to provide a good measurement. As the signal produced by the sensor has very low amplitude and is also susceptible to noise, it is necessary, on the one hand, to ensure noise immunity, which can be accomplished through a cable with a mesh connected to earth and, on the other hand, to guarantee amplification of the signal, using operational amplifiers. The implementation of filters, which will limit the signal measurement band, excludes unwanted frequencies, promoting a good signal-to-noise ratio.

The design of the signal conditioning circuit begins with the design of a second-order low-pass Chebyshev filter with a cutoff frequency of 1 kHz. This value was defined for the cut-

off frequency, considering the frequencies expected to provide information about the condition of the induction motor bearings. The spectral frequencies associated with typical bearing failures are usually below 1 kHz, which is why the spectrum was limited. In any case, other types of faults in electric motors tend to occur at low frequencies, so a low-pass filter with a very high cut-off frequency is not justified. The filter is implemented resorting to a TL062ACDT operational amplifier with field effect transistor (JFET) junction, in order to accomplish low power consumption.

Figure 11 illustrates the filter circuit, implemented in a computer simulation, using the MULTISIM software.

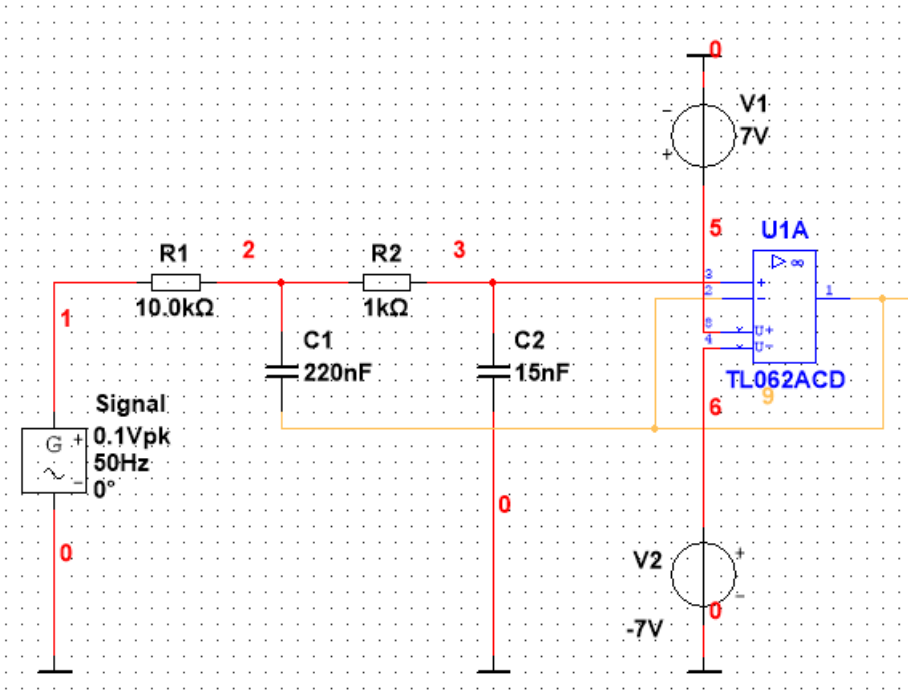

Figure 11 - Simulation of the second-order low-pass Chebyshev filter in MULTISIM.

The low-pass filter transfer function can be derived from Kirchhoff's law equations, defined in (19) - (22):

$$V_i(s) = R_1 I_1 + R_2 I_3 + \frac{1}{sC_2} I_4 \tag{19}$$

$$V_o(s) = \frac{V_i}{sC_2} I_4 \tag{20}$$

$$R_2 I_3 = \frac{1}{sC_1} I_2 \tag{21}$$

$$I_3 = I_4 \tag{22}$$

Combining (19) with (22) results in the transfer function (23):

$$\frac{V_o(s)}{V_i(s)} = \frac{1}{s^2 R_1 R_2 C_1 C_2 + s C_2 (R_1 + R_2) + 1} \tag{23}$$

The transfer function in (23) allows to define the filter parameters, as in (24) and (25):

$$R_1 R_2 C_1 C_2 = \frac{1}{\omega_n^2} \tag{24}$$

$$C_2 (R_1 + R_2) = \frac{2\delta}{\omega_n} \tag{25}$$

Using the appropriate MATLAB function for the chosen filter, theoretical values for the capacitances were obtained for pre-defined resistances of 10 kΩ and 1 kΩ, for R1 and R2, respectively. The theoretical capacitances were $C_1 = 2{,}07 \times 10^{-7}$F and $C_2 = 1{,}427 \times 10^{-8}$ F.

The filter was then implemented with capacitance values matching those available on the market, that is, C1 = 220 nF and C2 = 15 nF. The MATLAB simulation allowed us to compare the attenuation differences between the theoretical filter and the real filter. The similarity in response of both theoretical and practical filters, shown in Figure 12, confirms the feasibility of the selected resistances and capacitances.

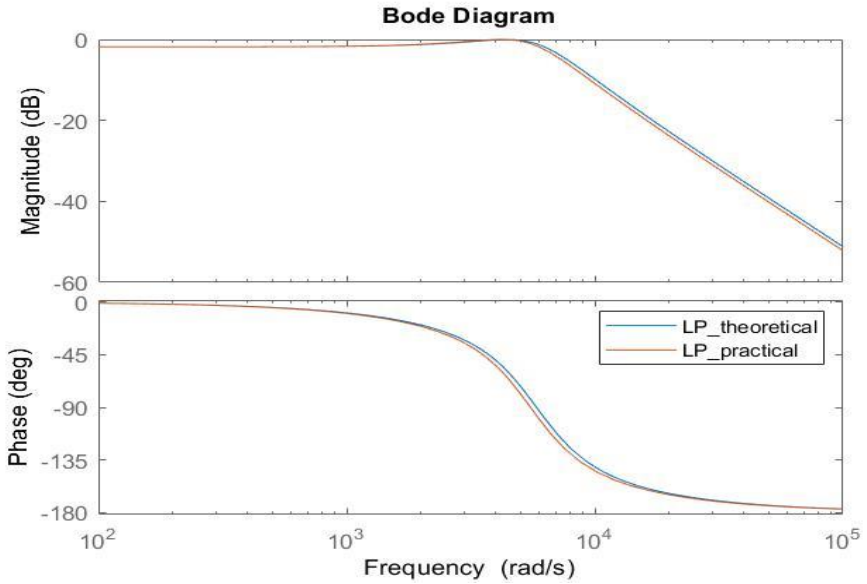

Figure 12 - Bode diagram of the designed low pass filter.

After designing the low-pass filter, a circuit was designed to compensate offset and amplify the signal, using the same operational amplifier to optimise space when designing the PCB. The offset compensation circuit is necessary to centre the signal from the accelerometer around the average value admitted by the microcontroller. The ESP32 inputs only read signals with voltages between 0 V and 3.3 V. Therefore, the value of the DC offset component is around 1.5 V.

The calculations for sizing the offset compensation circuit [19] depend on the theoretical values of the circuit for the gain and offset. The following parameters are initially defined for the circuit design:

- The voltage level of a stable reference, Vref = 1.500 V
- The full-scale output voltage, VoutFS = 3.300 V
- The zero-scale output voltage, VoutZS = 0.035 V
- The full-scale input voltage, VinFS = 0.100 V
- The zero-scale input voltage, VinZS =0.001 V

The calculation of the offset stage and gain was obtained taking the previous values as a starting point, and determined according to the following equations [19]:

$$m = \frac{V_{out}fs - V_{out}zs}{V_{in}fs - V_{in}zs} \tag{26}$$

$$b = V_{out}zs - m \times V_{in}zs \tag{27}$$

where *"m"* corresponds to the stage gain and *"b"* the stage offset.
The circuit with the operational amplifier designed for the necessary gain and offset requirements follows the configuration shown in Figure 13, since both *"m"* and *"b"* have a positive sign.

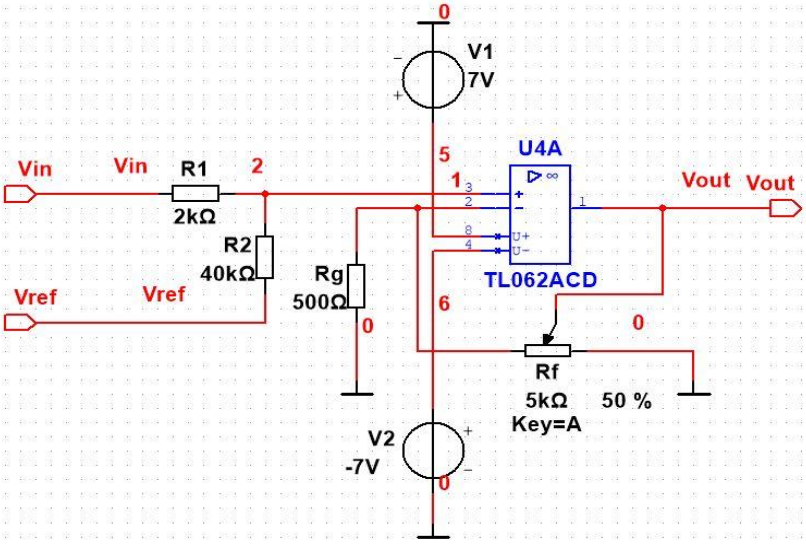

Figure 13 - Schematic diagram of the amplification stage.

A potentiometer was placed at *"Rf"* to allow adjustment of the circuit gain. The value of R1 was adjusted empirically until the value of the output signal in *"Vout"* was obtained within the desired voltage range.

According to the accelerometer datasheet [12], the sensitivity value for 1 g is 100 mV. Accordingly, the simulation of the entire signal conditioning circuit emulates the accelerometer response using a signal generator with a 100 mV peak voltage. Figure 14 illustrates the result of joining the filtering circuit with the respective offset and gain compensation circuit.

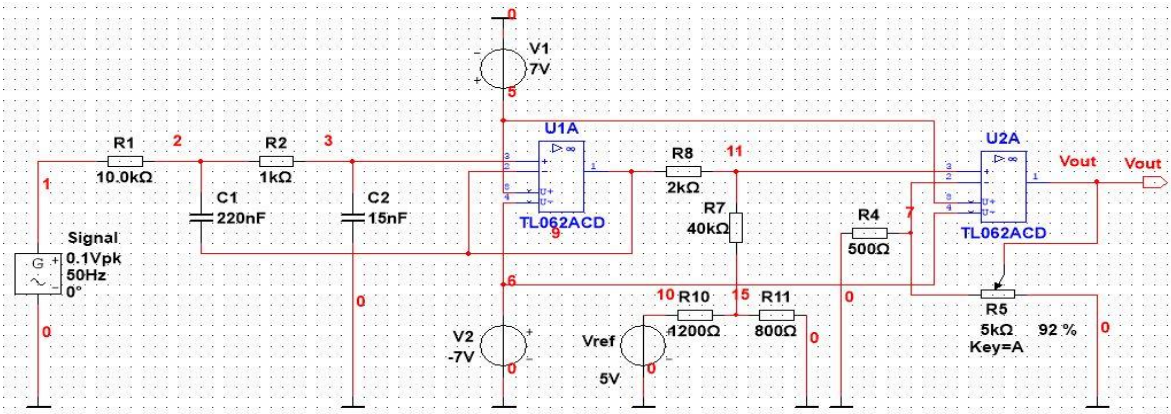

Figure 14 - Accelerometer signal conditioning circuit.

Figure 15 shows the signals at two distinctive points of the signal conditioning circuit. In orange, the signal at the output of the low-pass filter and in red the signal at the output of the signal conditioning circuit. When analysing the circuit response, it is confirmed that the conditioned signal undergoes a significant increase in amplitude and oscillates around an average value of 1.5 V, remaining within allowable voltages for the ESP32 microcontroller.

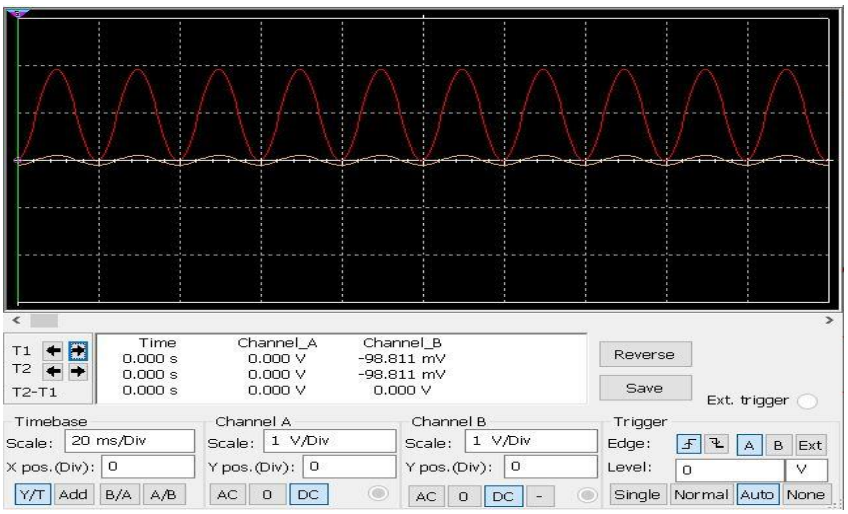

Figure 15 - Visualisation of the signal before the offset gain stage (orange) and after amplification (red).

The PCB design, which includes the all the signal conditioning capabilities and the microcontroller, can be consulted in the appendix of the dissertation.

Chapter 4

Experimental results

This chapter describes the adopted methodology, as well as the setup used to carry out the experimental tests. During the testing phase, the design of the signal conditioning circuit did not integrate the offset compensation circuit, having been subject to several optimizations, which is why the results presented below show the signal in the time domain around 0 V, i.e., without offset. At the end of the chapter, an analysis of the results obtained under the different test conditions is presented.

4.1. Experimental setup and equipment

To test the effectiveness of the platform designed to monitor vibrations in induction motors, an experimental setup was created at the Laboratory of Electromechatronic Systems (CISE | LSE). Figure 16 illustrates the laboratory setup used to carry out the experimental tests.

The scheme begins with the autotransformer connected to the laboratory's three-phase power supply, which supplies 400 V to the WEG three-phase induction motor with squirrel cage rotor, model W22. This motor is mechanically coupled to a hysteresis dynamometer, the HD-815-8NA, which in turn is controlled by the DSP 7000 device. This controller allows to precisely control the applied load torque. Three accelerometers coupled to a magnetic base, are placed on the motor drive end, in three distinct axes (vertical, horizontal, and axial) in relation to the rotor axis. The accelerometer is connected to the signal conditioning board. Using a symmetrical power supply, the operational amplifiers are powered and the Agilent DSOX2014A oscilloscope is connected to the output of the signal conditioning circuit, collecting data measured in both the time and frequency domains.

The tests were carried out in two stages. To establish the baseline for comparison, vibration analysis is conducted with a healthy motor condition, operating in three load torque conditions: 1) no load (0.1 Nm); 2) half load (7 Nm, 1 kW); and 3) full load (14 Nm, 2.110 kW). In the second stage, vibration analysis is conducted considering bearing fault conditions, for the same three load torque conditions. In each test, vibration is monitored in the three axes, recording data for each of the axis.

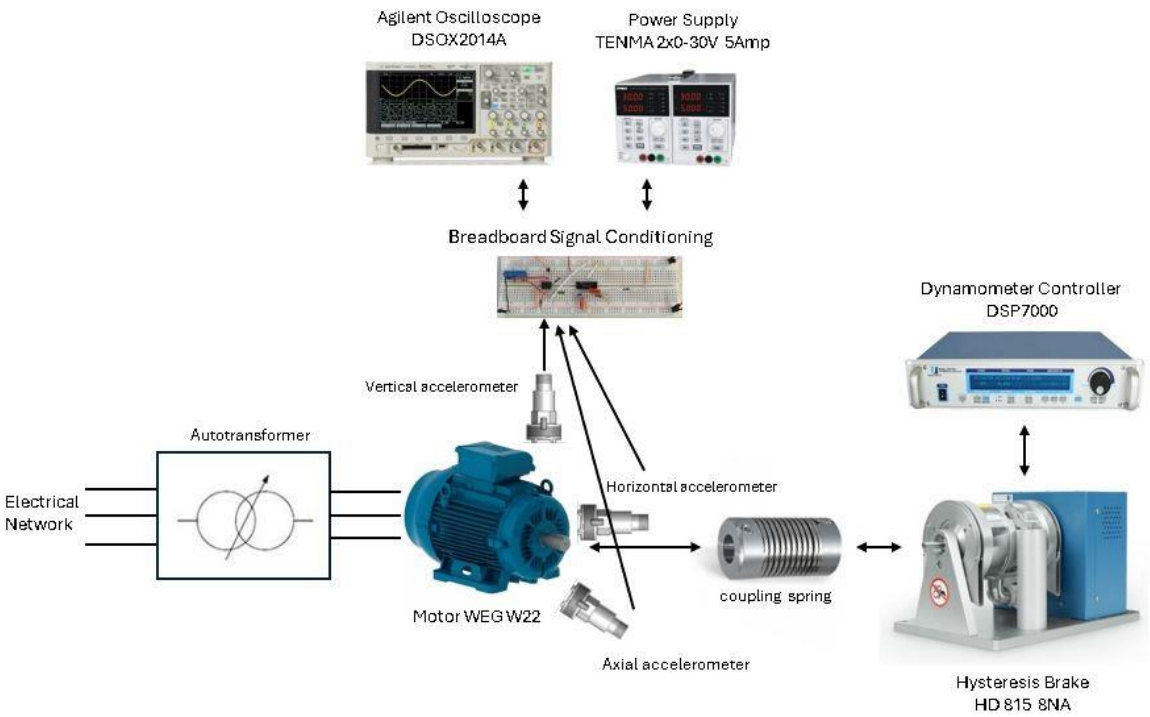

Figure 16 - Laboratory setup for testing the accelerometer signal conditioning system.

4.2. Motor test with healthy bearing

The first test aims to collect vibration data from a motor that is in perfect operating condition. It is known that its bearing is still in the initial phase of operating time, without damage or wear. Figure 17 shows the conditioned output signal, obtained from the vertical axis accelerometer, with the motor operating at a speed of 1500 revolutions per minute (RPM), without load torque.

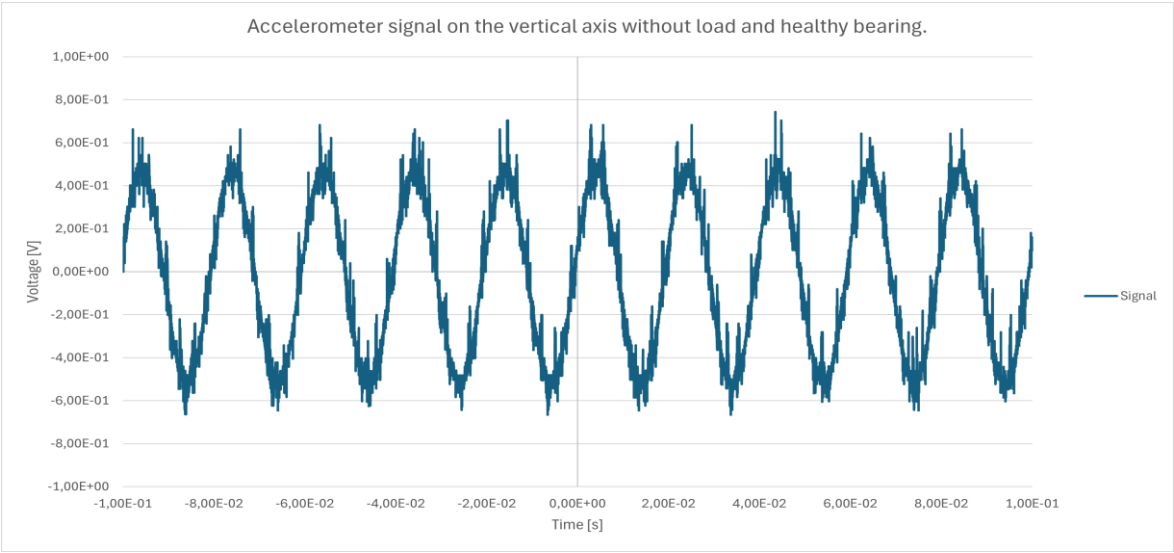

Figure 17 – Output signal of the vertical axis accelerometer, without load torque.

Figure 18 shows the response, in the frequency domain, of the same accelerometer. Clearly, the 50 Hz harmonic stands out from all others. The presence of other harmonics is residual.

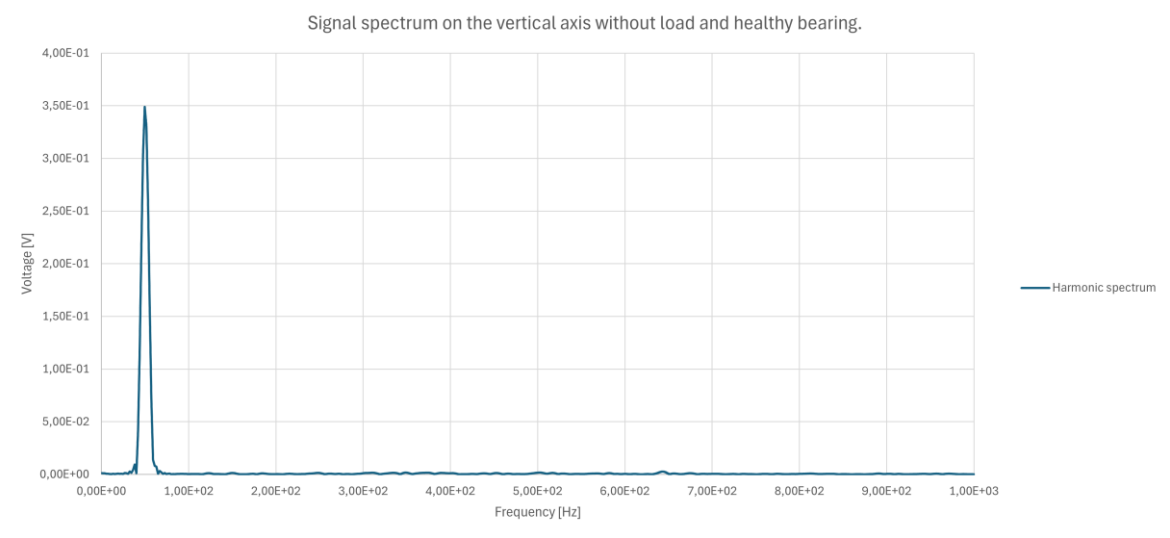

Figure 18 - Signal spectrum of the vertical axis accelerometer output, without load torque.

Figure 19 shows the conditioned output signal, obtained on the horizontal axis, with the motor operating at a speed of 1500 RPM, without load torque.

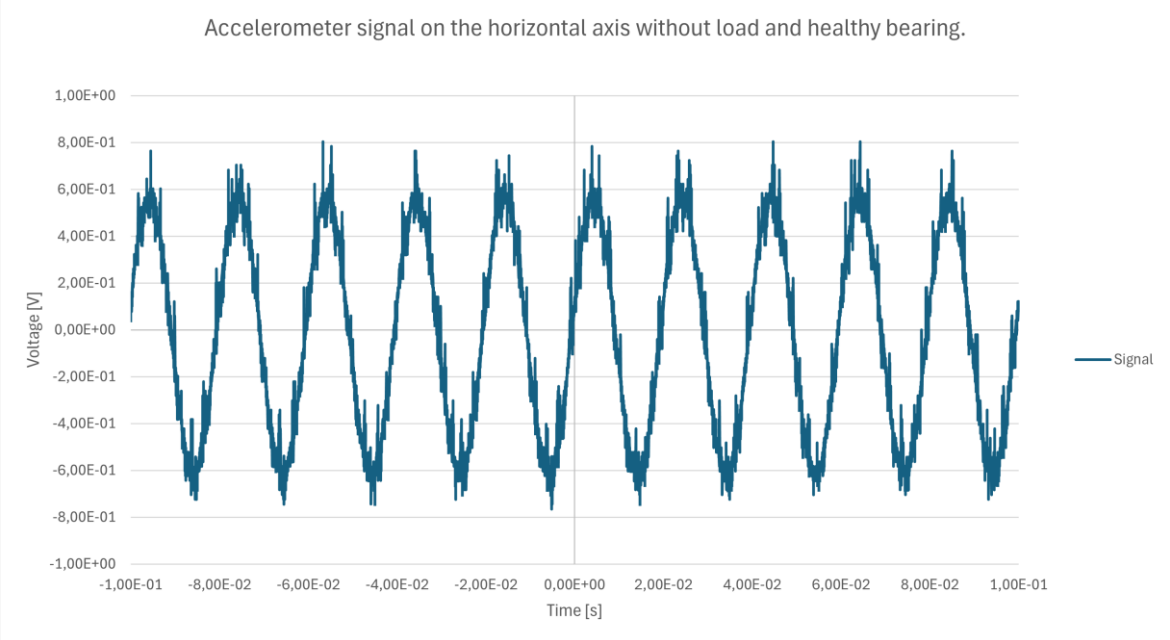

Figure 19 – Output signal of the horizontal axis accelerometer, without load torque.

Figure 20 shows the response, in the frequency domain, of the same accelerometer. Likewise, the 50 Hz harmonic stands out from all others. The presence of other harmonics is also residual in the horizontal axis.

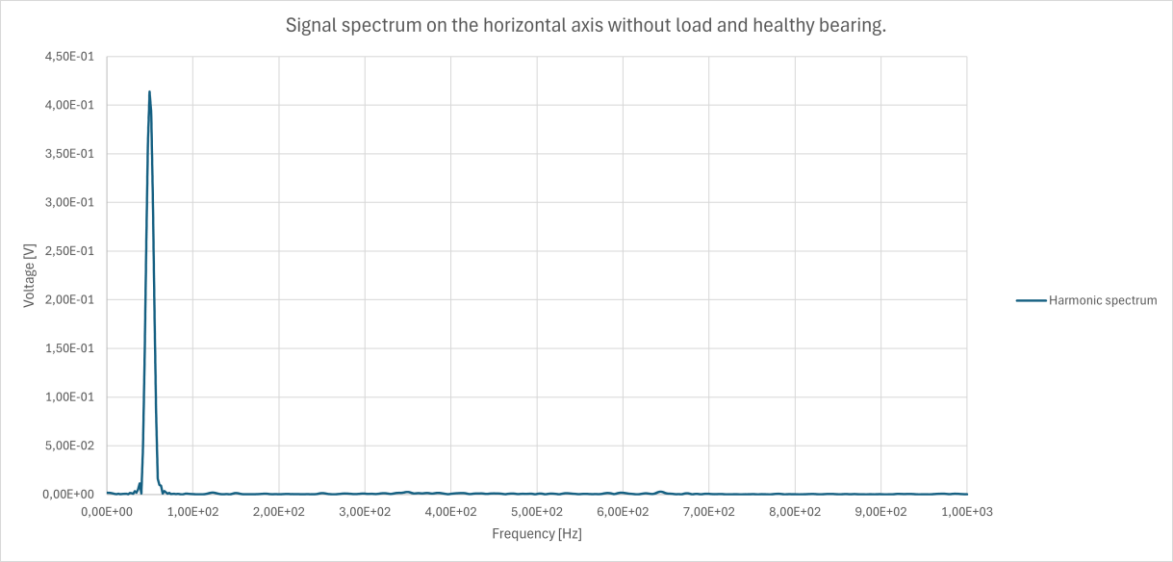

Figure 20 - Signal spectrum of the horizontal axis accelerometer output, without load torque.

Finally, Figure 21 and Figure 22 show the conditioned output signal obtained on the axial axis, represented in the time and frequency domains, respectively, with the motor operating in healthy condition and without load torque.

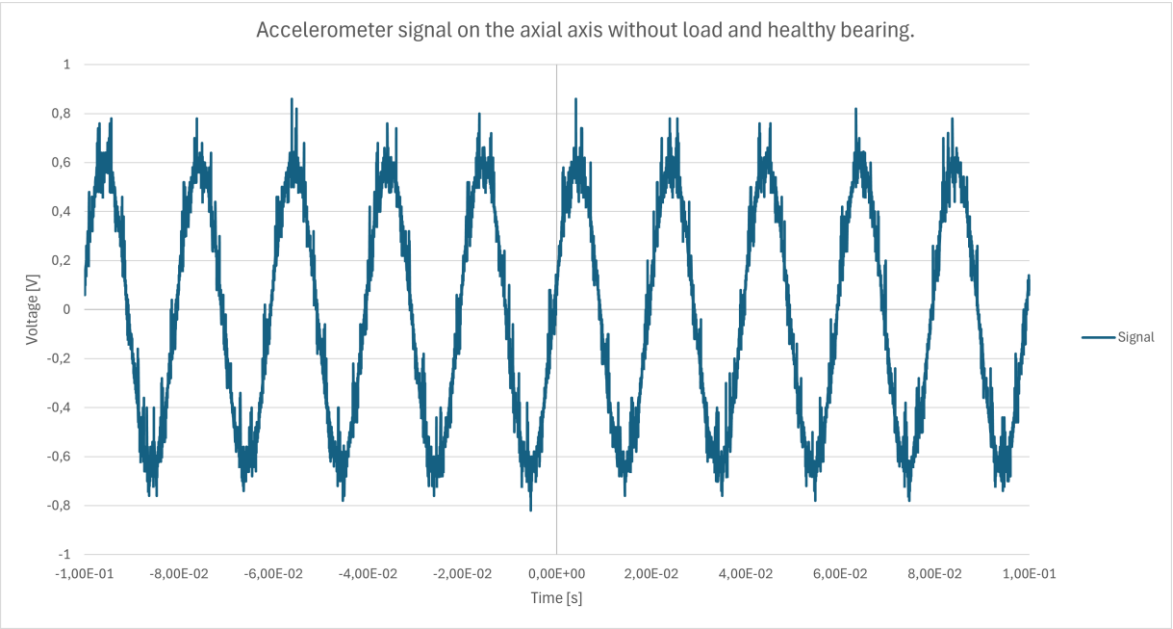

Figure 21 – Output signal of the axial axis accelerometer, without load torque.

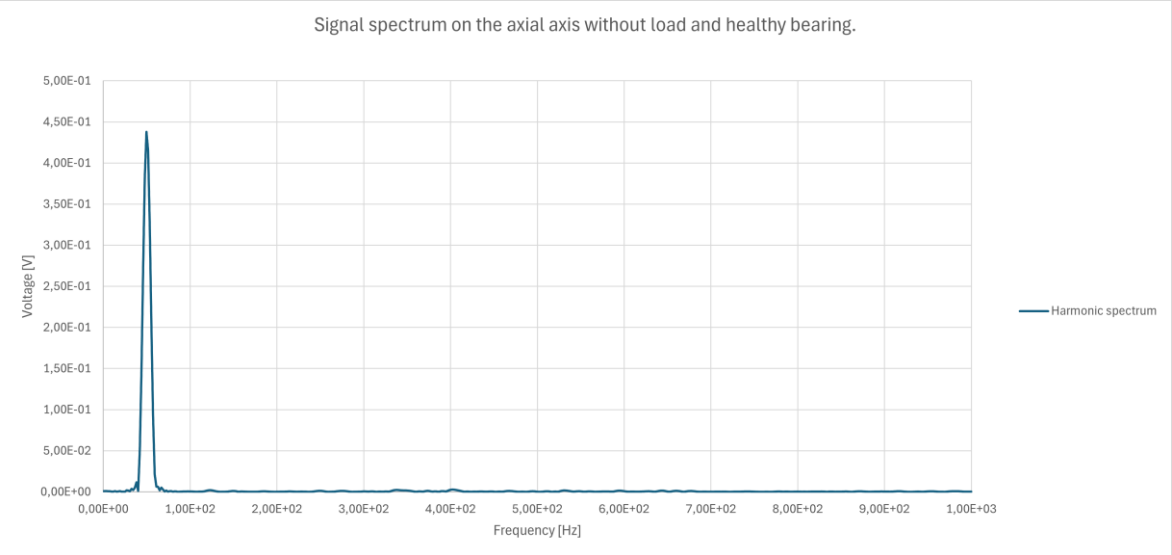

Figure 22 – Signal spectrum of the axial axis accelerometer output, without load torque.

After obtaining the experimental results for no load conditions, the test procedure was repeated, now considering a load torque of 7 Nm, which led to a mechanical speed of 1473 RPM. Figure 23 illustrates the conditioned output signal, again with the accelerometer placed on the vertical axis, with the motor operating at half load.

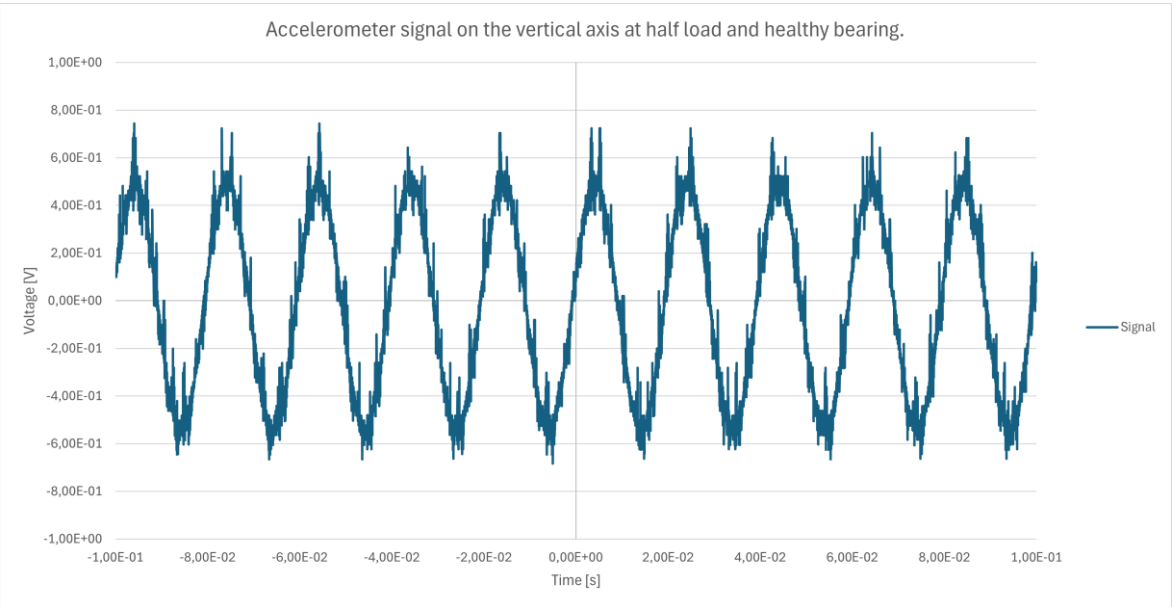

Figure 23 - Output signal of the vertical axis accelerometer, under half load torque condition.

Figure 24 shows the response, in the frequency domain, of the same output. Likewise, the 50 Hz harmonic stands out from all others.

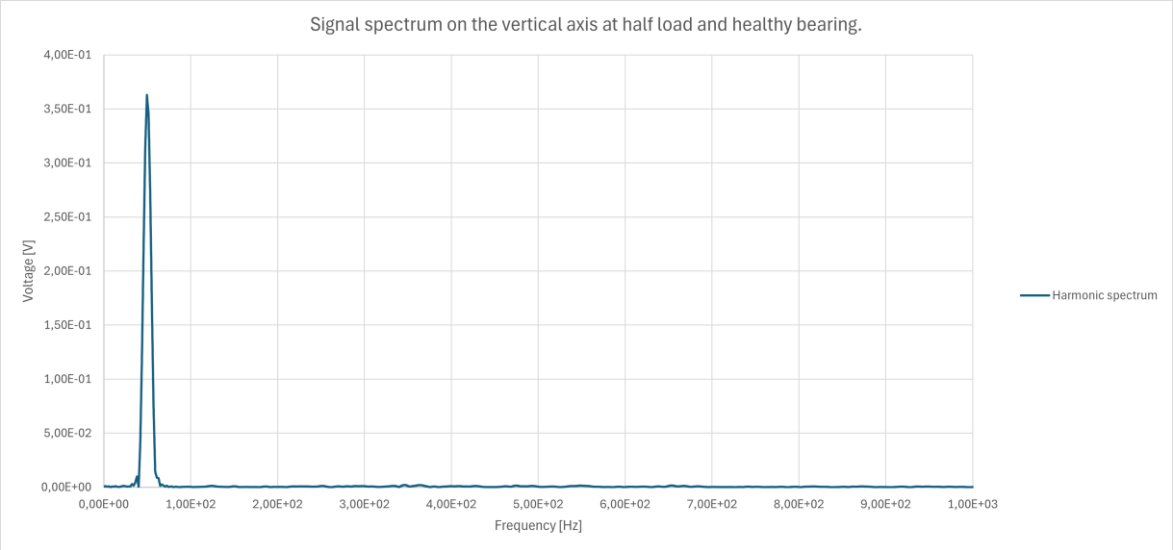

Figure 24 - Signal spectrum of the vertical axis accelerometer output, at half load.

Figure 25 shows the output signal, obtained on the horizontal axis, with the motor operating at a speed of 1473 RPM, at half load.

Figure 25 – Output signal of the horizontal axis accelerometer, at half load.

Figure 26 shows the response, in the frequency domain, of the same output.

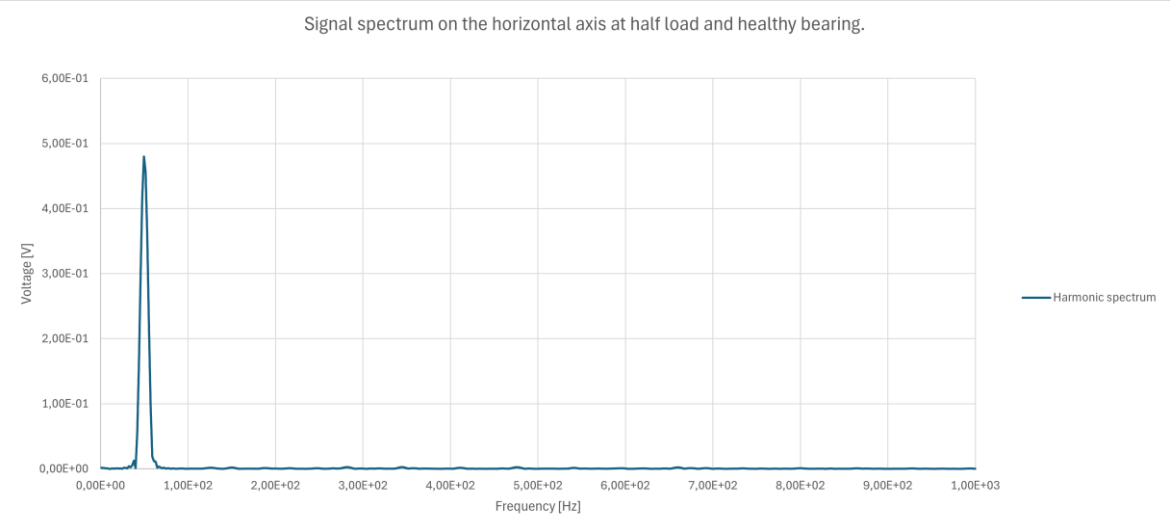

Figure 26 - Signal spectrum of the horizontal axis accelerometer output, at half load.

Figure 27 and Figure 28 show the signals obtained on the axial axis, in the time and frequency domains, with the motor operating in healthy condition and half load torque.

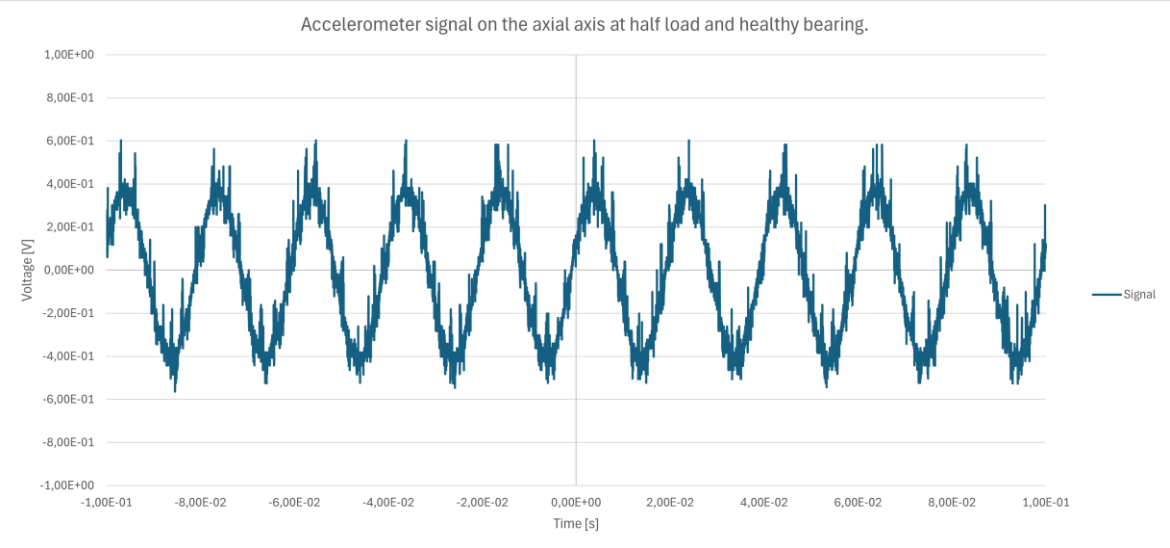

Figure 27 - Output signal of the axial axis accelerometer, at half load.

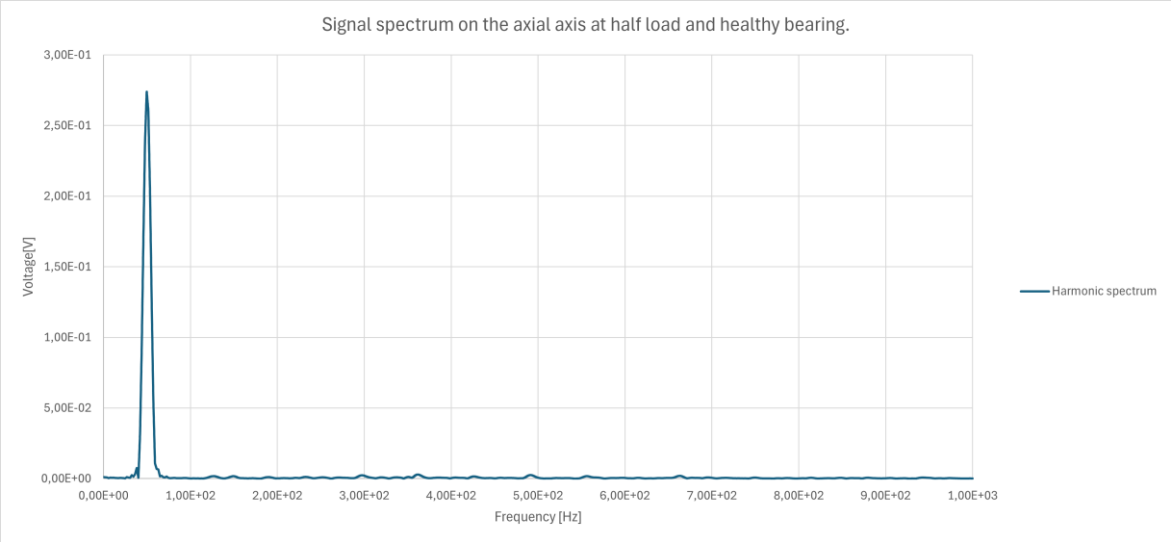

Figure 28 - Signal spectrum of the axial axis accelerometer output, at half load.

After obtaining the experimental results for half load conditions, the test procedure was repeated, now considering the rated load torque of the tested motor (14 Nm), which led to a mechanical speed of 1442 RPM. Figure 29 and Figure 30 illustrate the conditioned output signal, in the time and frequency domains, again with the accelerometer placed on the vertical axis, with the motor operating at full load.

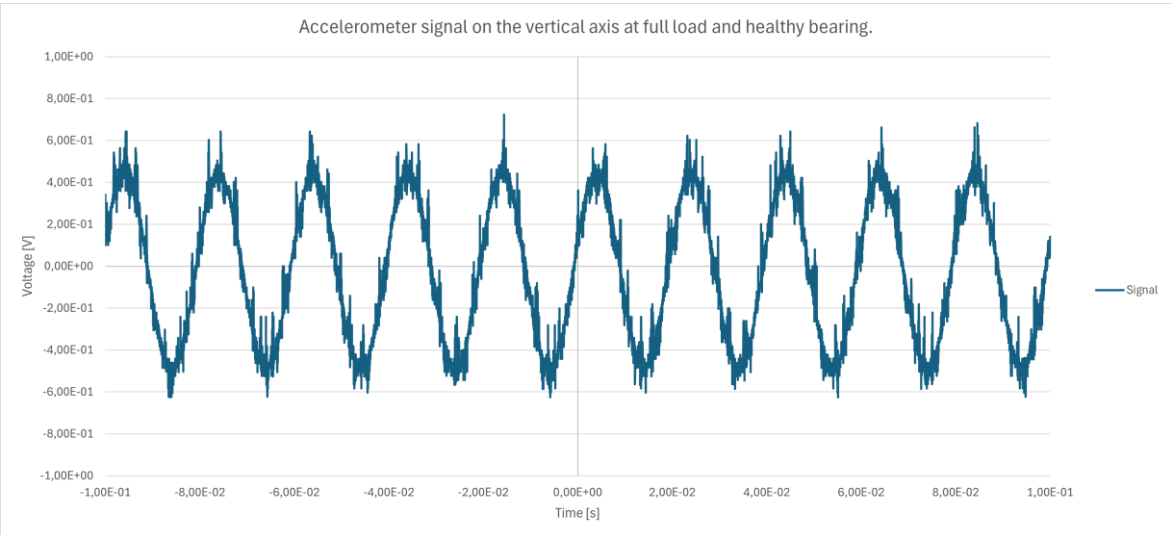

Figure 29 – Output signal of the vertical axis accelerometer, at full load torque.

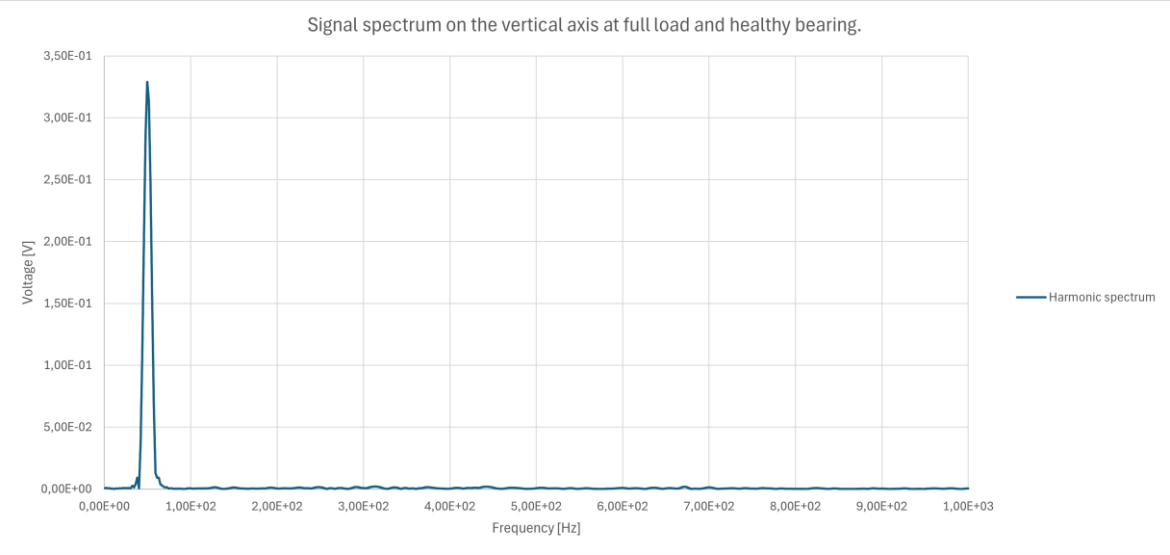

Figure 30 - Signal spectrum of the vertical axis accelerometer output, at full load.

Figure 31 and Figure 32 show the conditioned signal, represented in the time and frequency domains, respectively, obtained on the horizontal axis accelerometer with the motor operating at full load.

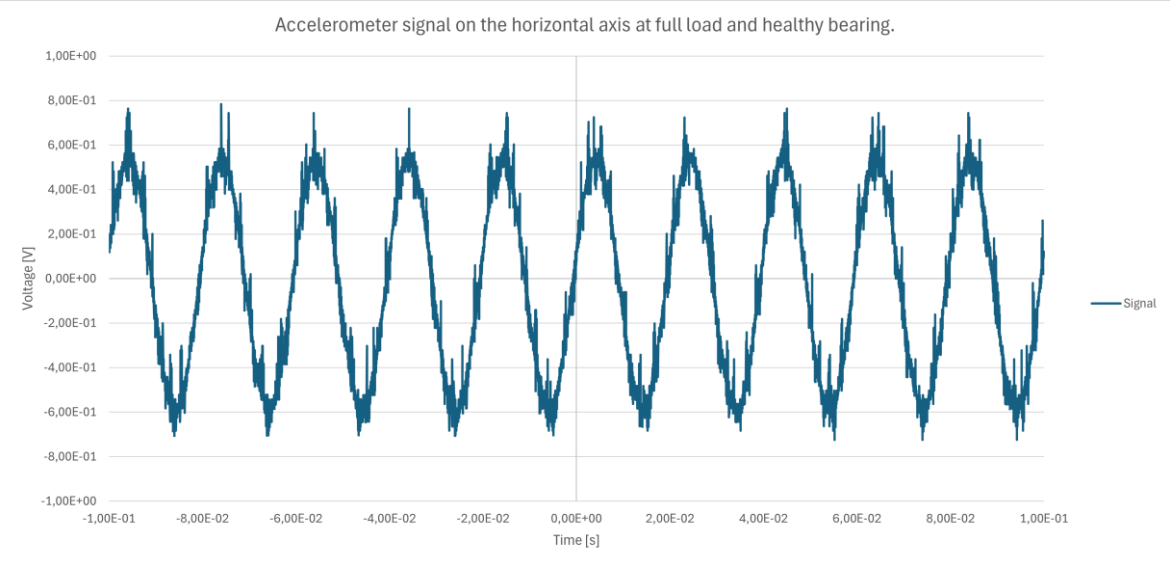

Figure 31 - Output signal of the horizontal axis accelerometer, at full load.

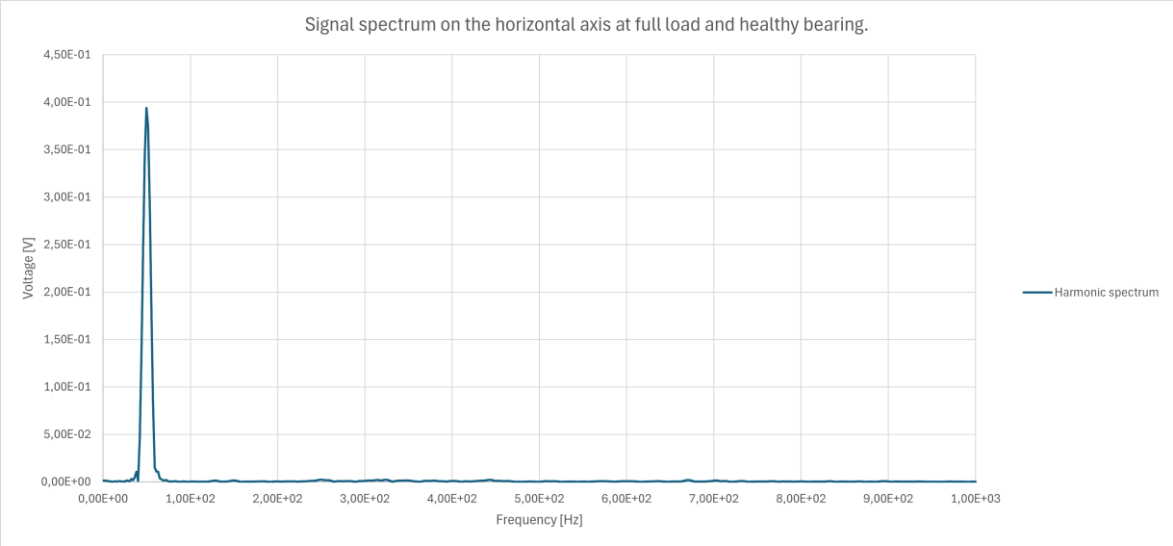

Figure 32 - Signal spectrum of the horizontal axis accelerometer output, at full load.

Completing the testing phase of the healthy motor, Figure 33 and Figure 34 show the signals obtained on the axial axis, in the time and frequency domains, with the motor operating at full load torque.

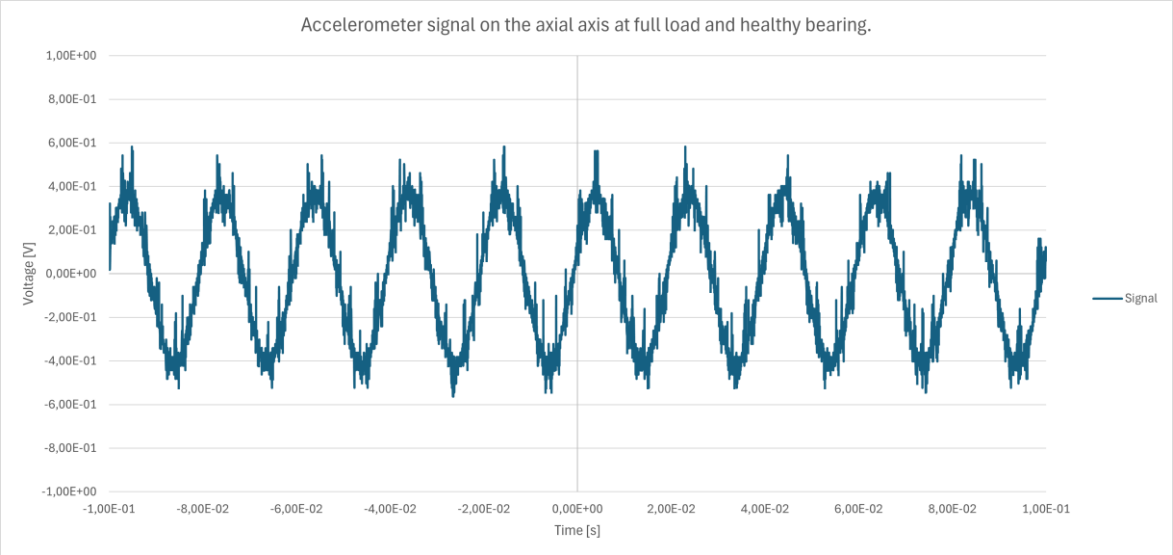

Figure 33 - Output signal of the axial axis accelerometer, at full load.

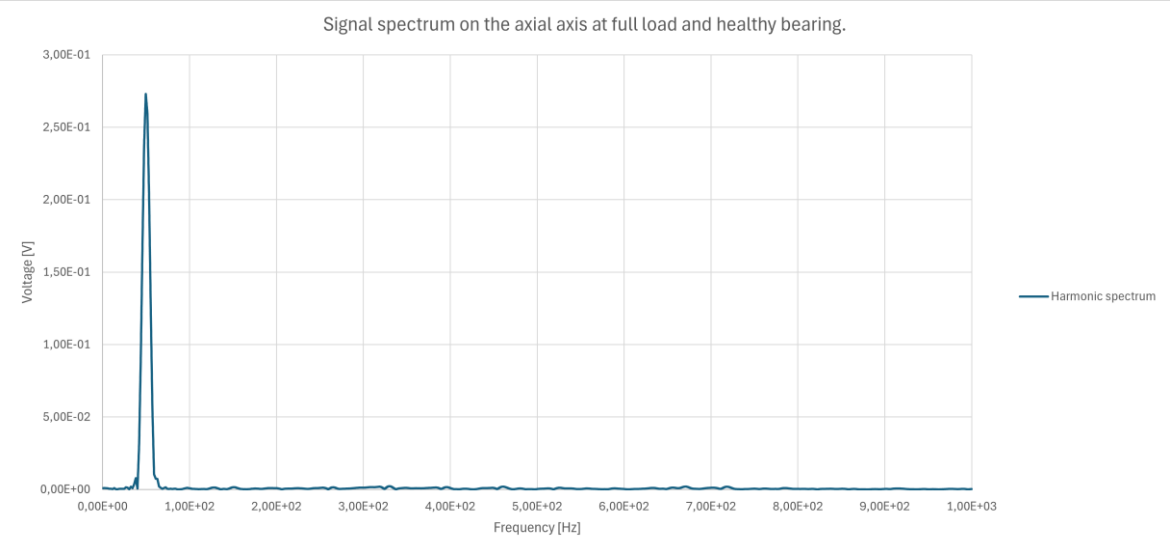

Figure 34 - Signal spectrum of the axial axis accelerometer output, at full load.

In conclusion, all results present a relevant degree of similarity. The amplitude of the 50 Hz harmonic stands out from all others, while the remaining harmonics show residual amplitudes. This suggests that the vibration profile remains uniform over the entire load range and for the three axis being monitored.

4.3. Motor testing with damaged bearing

The second set of tests aims to collect vibration data from an induction motor operating with a faulty bearing. A bearing with a 2 mm hole in the outer race was placed on the rotor shaft, on the drive end. For an effective comparison of scenarios, the motor with the faulty bearing is tested for the same three levels of load torque and speed. The similarity between test conditions should allow to diagnose the presence of the fault, its location and severity.

Figure 35 and Figure 36 show the conditioned signal obtained on the vertical axis accelerometer, in the time and frequency domains, with the motor operating at a speed of 1500 RPM, without load torque.

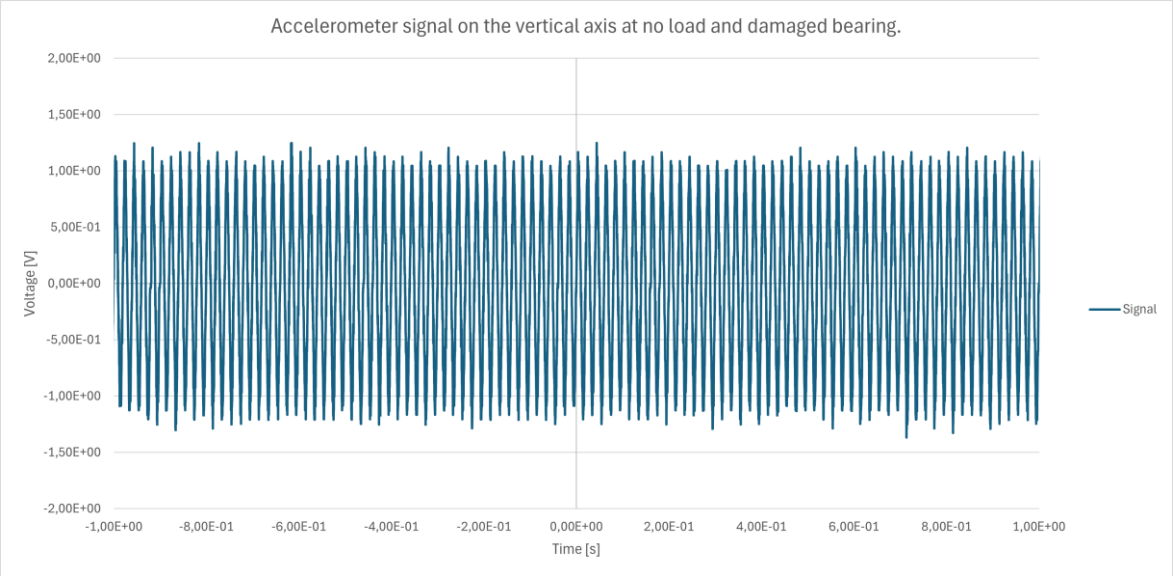

Figure 35 - Output signal of the vertical axis accelerometer, without load torque and damaged bearing on the outer race.

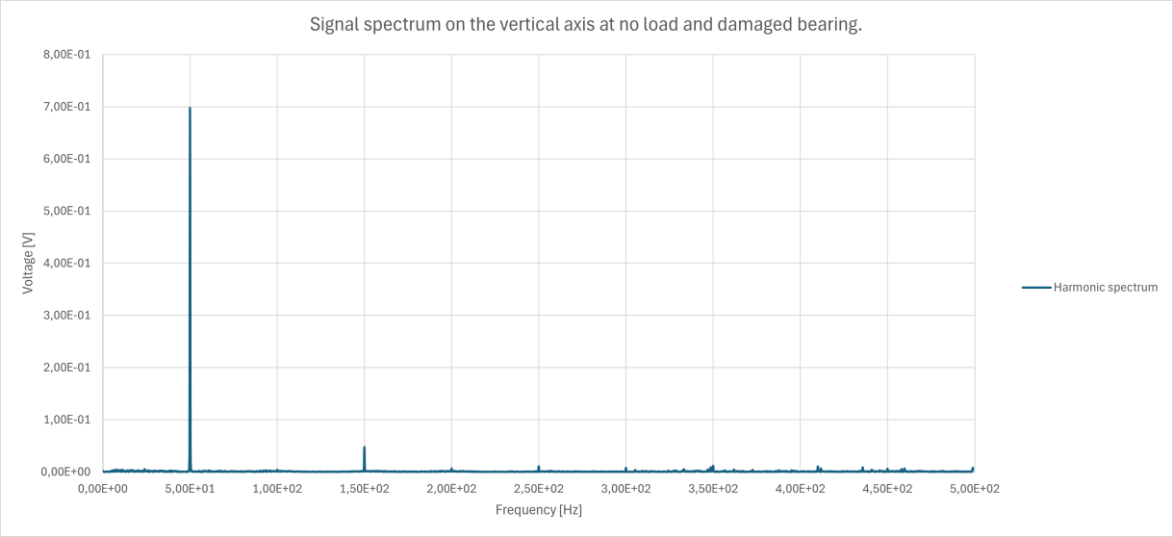

Figure 36 - Signal spectrum of the vertical axis accelerometer output, without load and damaged bearing on the outer race.

The results of Figure 37 and Figure 38 show the conditioned signal obtained on the horizontal axis accelerometer, in the time and frequency domains, with the motor operating at a speed of 1500 RPM, without load torque.

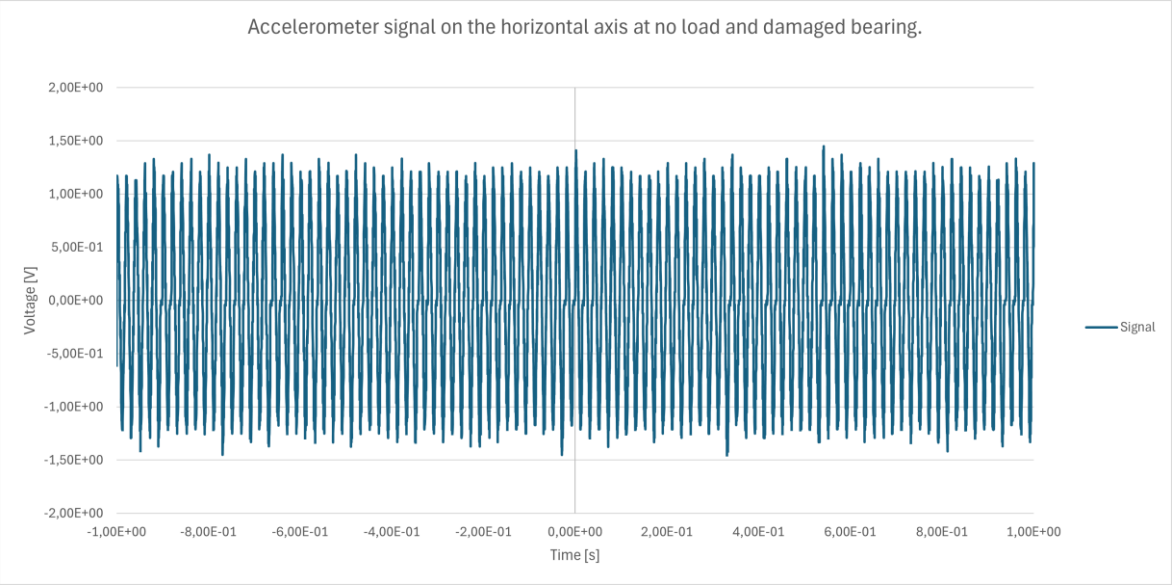

Figure 37 – Output signal of the horizontal axis accelerometer, without load torque and damaged bearing on the outer race.

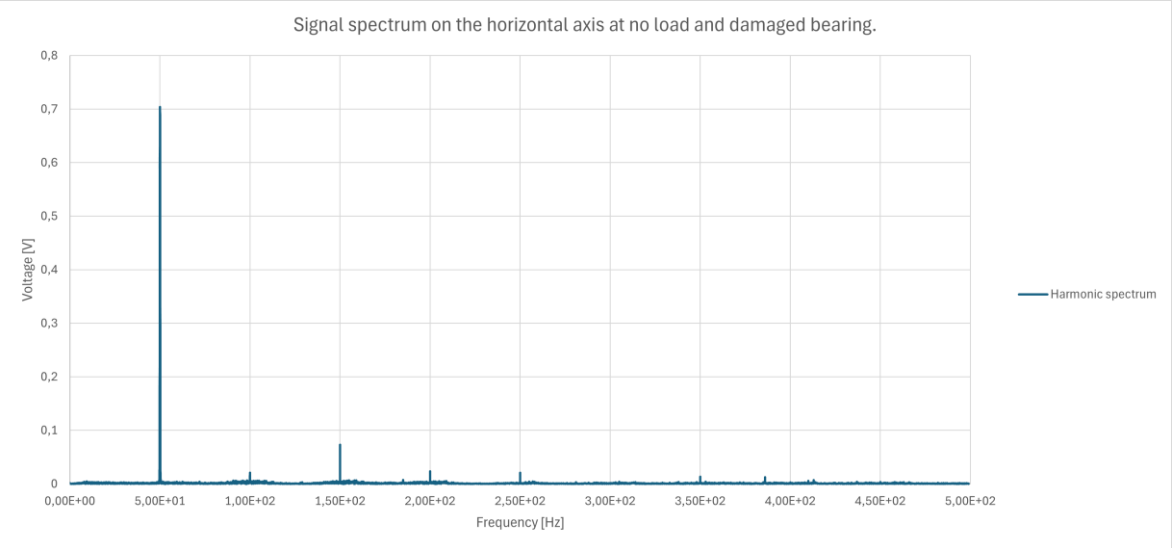

Figure 38 - Signal spectrum of the horizontal axis accelerometer output, without load and damaged bearing on the outer race.

Finally, Figure 39 and Figure 40 show the conditioned signal obtained on the axial axis accelerometer, in the time and frequency domains, with the motor operating at a speed of 1500 RPM, without load torque.

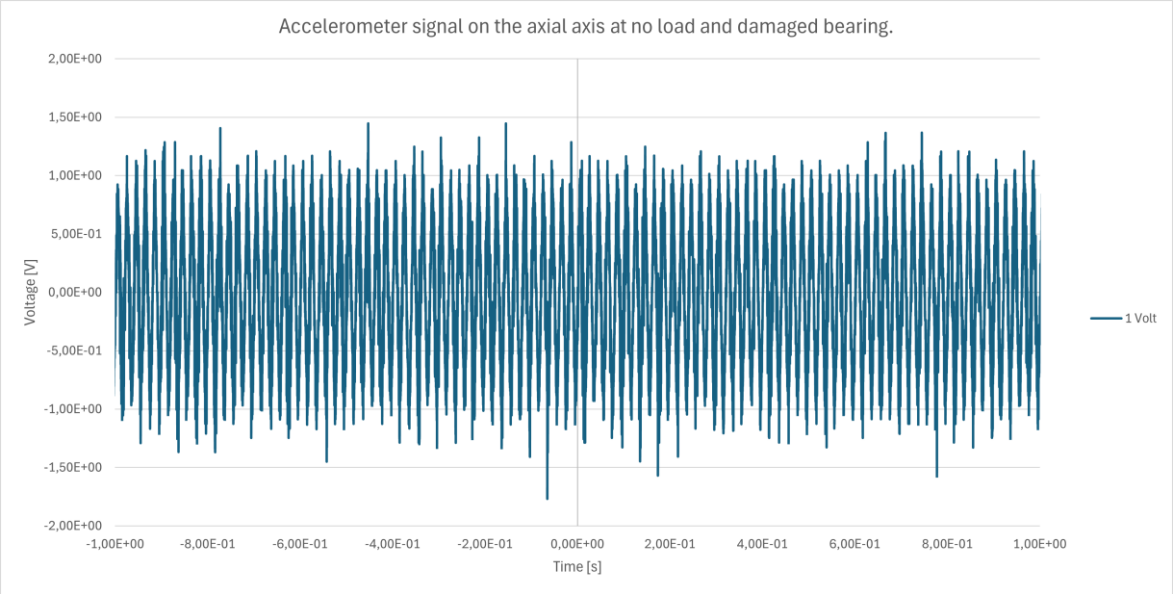

Figure 39 - Output signal of the axial axis accelerometer, without load and damaged bearing on the outer race.

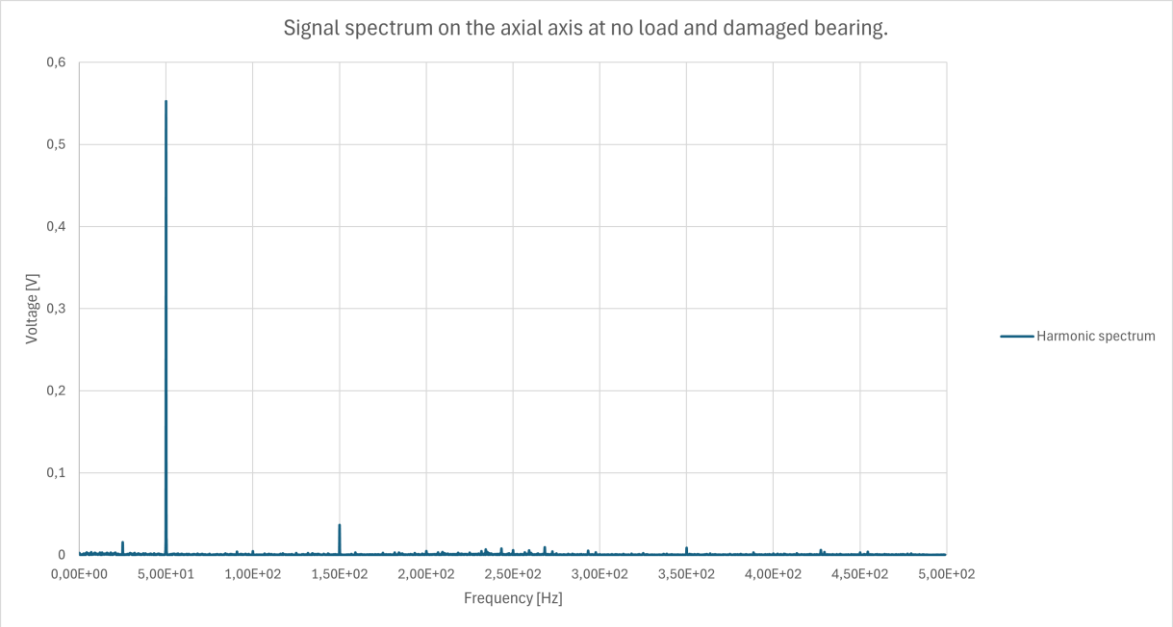

Figure 40 - Signal spectrum of the axial axis accelerometer output, without load and damaged bearing on the outer race.

As considered for healthy motor conditions, the hysteresis dynamometer was activated again to simulate a load torque of 7 Nm, leaving the motor operating at 1473 RPM. In this regime, half load operation is considered. Figure 41 and Figure 42 illustrate the conditioned signal obtained on the vertical axis accelerometer, in the time and frequency domains, with the motor operating at a half load torque.

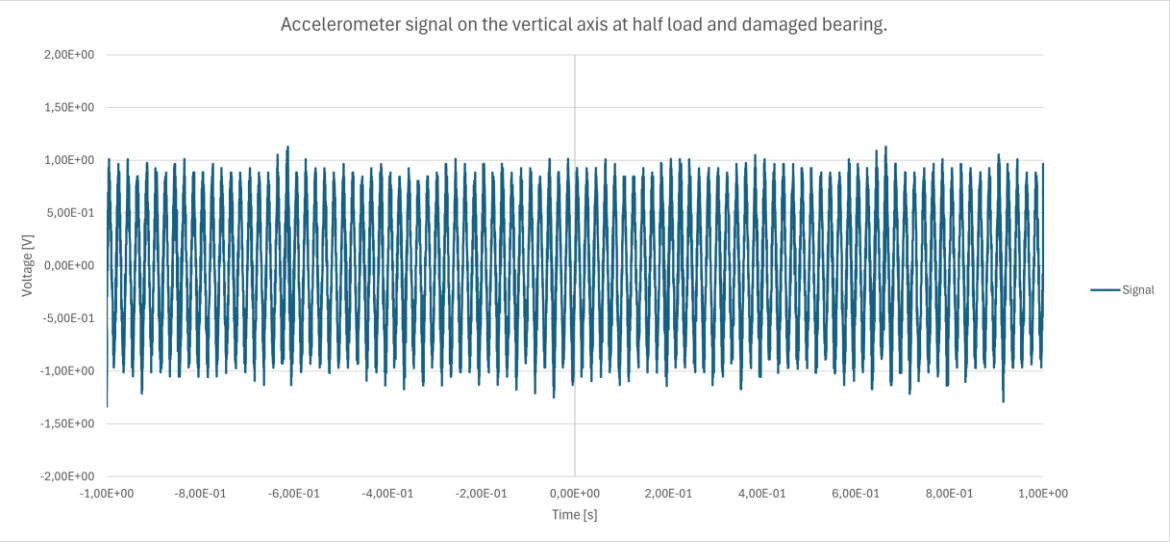

Figure 41 - Output signal of the vertical axis accelerometer, at half load condition and damaged bearing on the outer race.

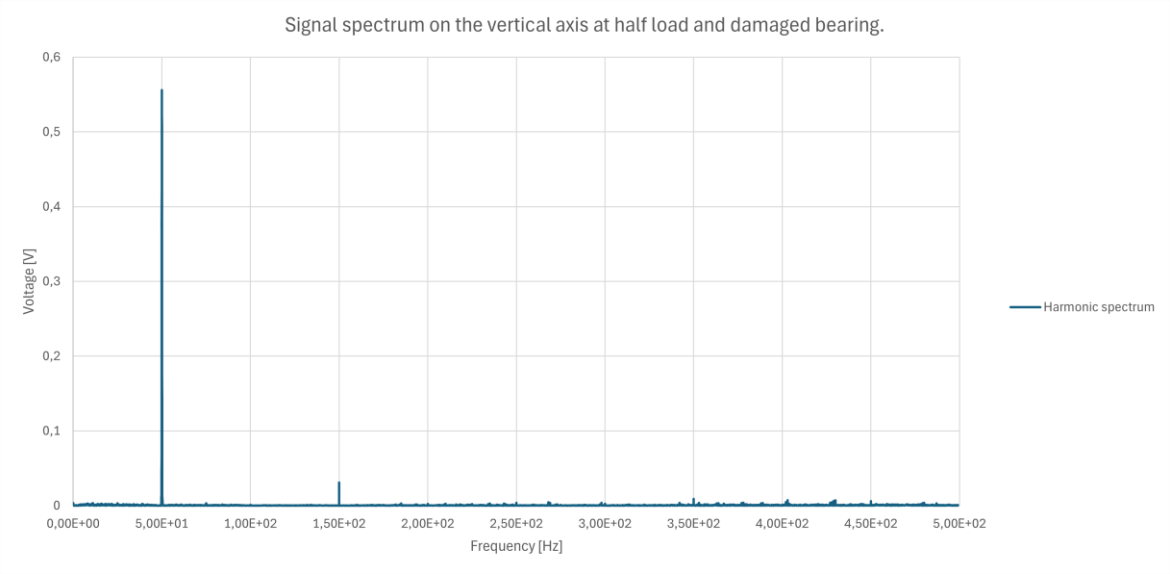

Figure 42 - Signal spectrum of the vertical axis accelerometer output, at half load condition and damaged bearing on the outer race.

The results of Figure 43 and Figure 44 show the conditioned signal obtained on the horizontal axis accelerometer output, represented in the time and frequency domains, with the motor operating at the same rotation speed as the previous test and with the same load torque.

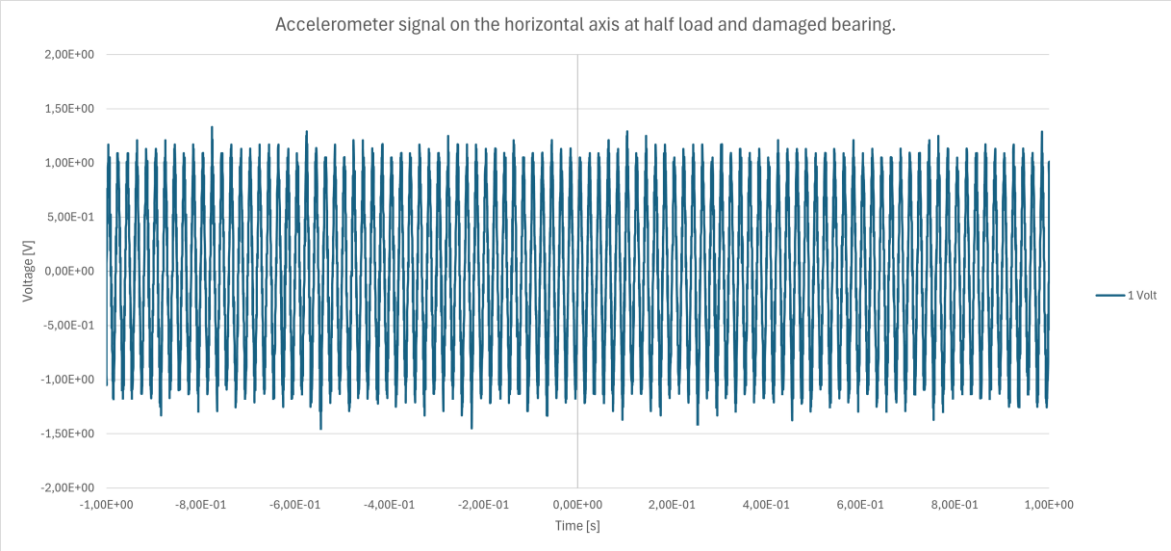

Figure 43 – Output signal of the horizontal axis accelerometer, at half load condition and damaged bearing on the outer race.

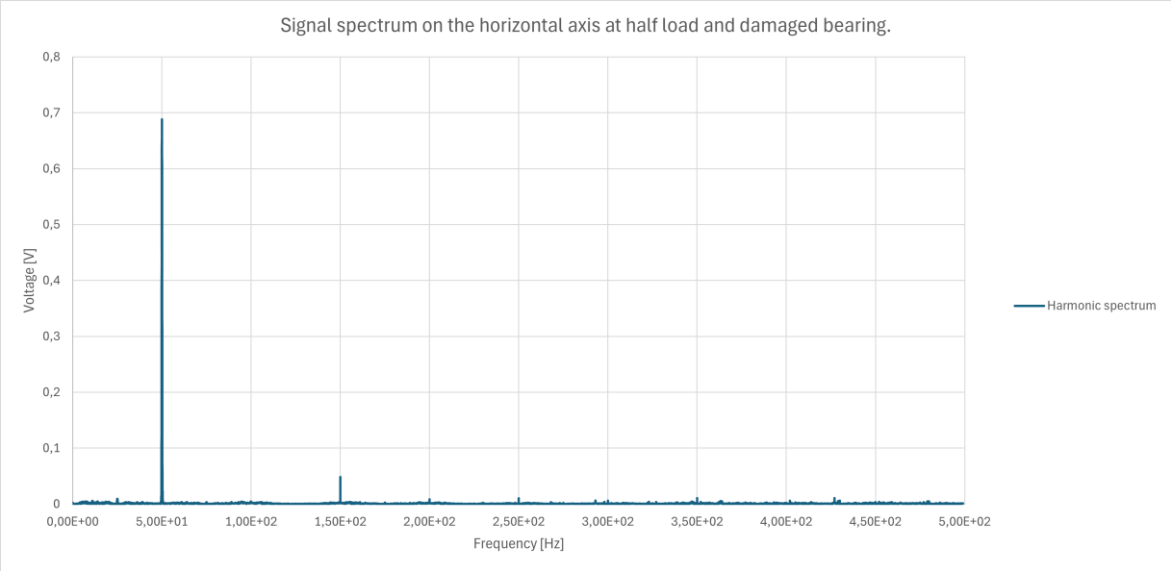

Figure 44 - Signal spectrum of the horizontal axis accelerometer output, at half load condition and damaged bearing on the outer race.

Finally, the results shown in Figure 45 and Figure 46 show the conditioned signal obtained on the axial axis, represented in the time and frequency domains, with the motor operating in the same regime as the previous results.

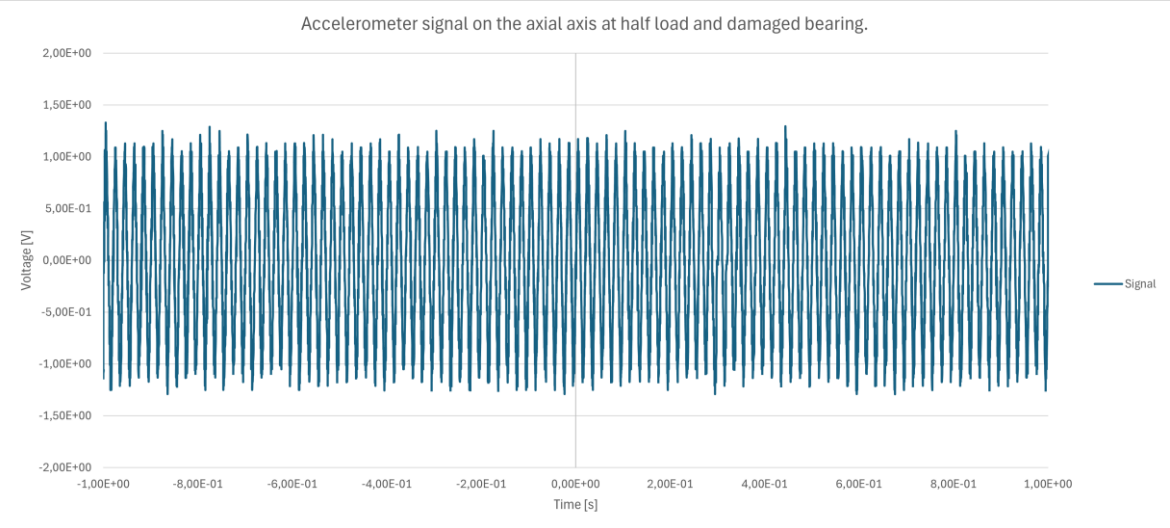

Figure 45 – Output signal of the axial axis accelerometer, at half load condition and damaged bearing on the outer race.

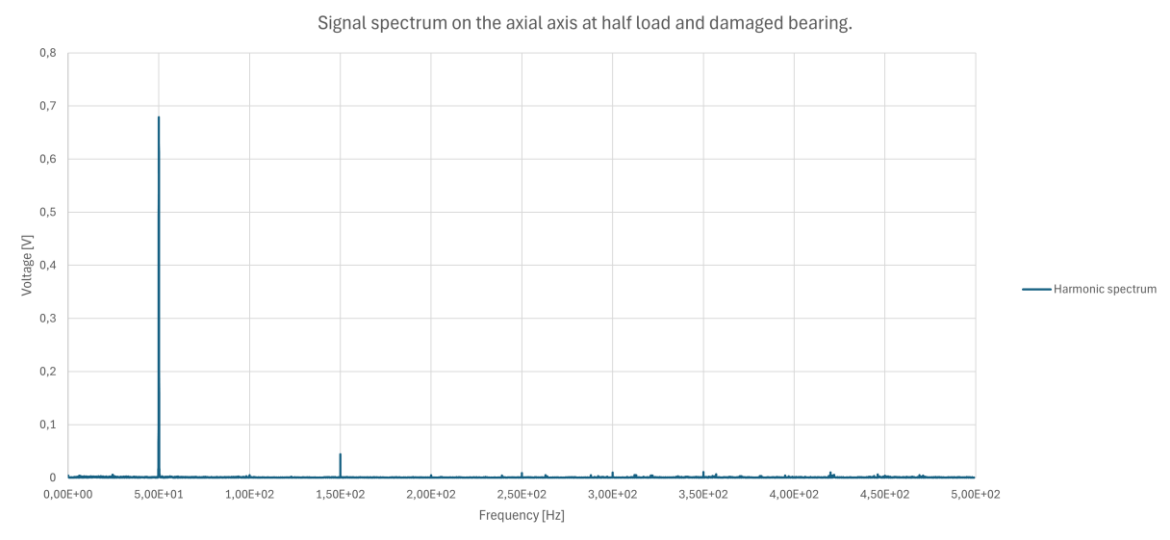

Figure 46 - Signal spectrum of the axial axis accelerometer output, at half load condition and damaged bearing on the outer race.

At the end of the battery of tests carried out with the motor operating under half load condition, the load torque was increased to the rated level, that is, 14 Nm, which represents a mechanical power of 2.113 kW. In this testing phase, the noise caused by the damaged bearing intensifies and it becomes quite evident that the engine is operating under adverse conditions. Despite that, it reveals considerable tolerance to failure, despite the high load torque to which it is subjected. The following results are part of the last battery of tests and illustrate the conditioned accelerometer signal, represented in the time and frequency domains. Adopting the same order of placement, the analysis starts with the vertical axis.

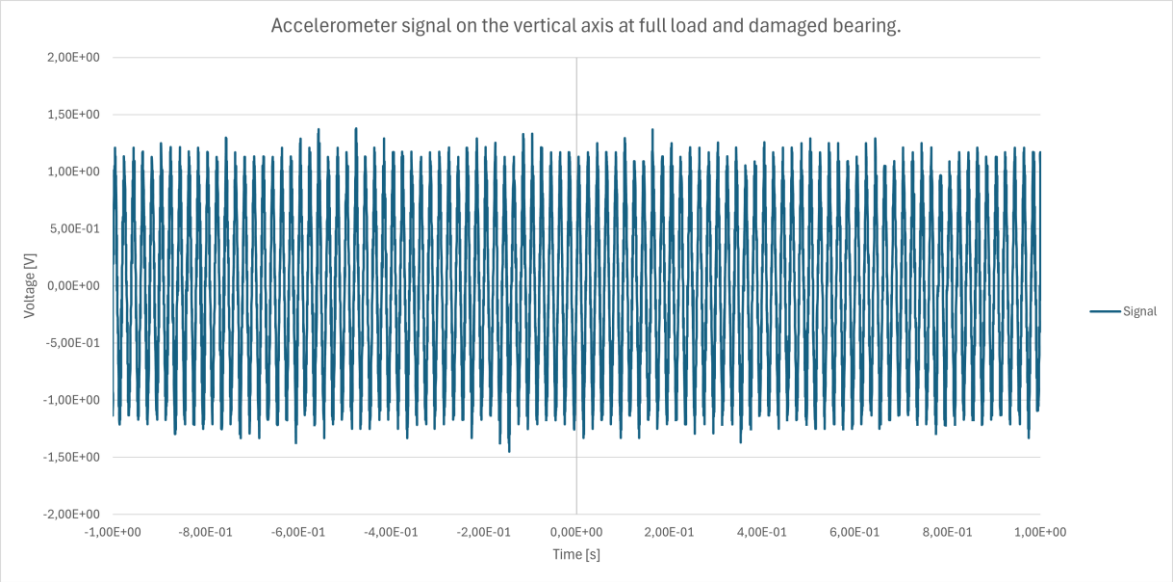

Figure 47 – Output signal of the vertical axis accelerometer, at full load condition and damaged bearing on the outer race.

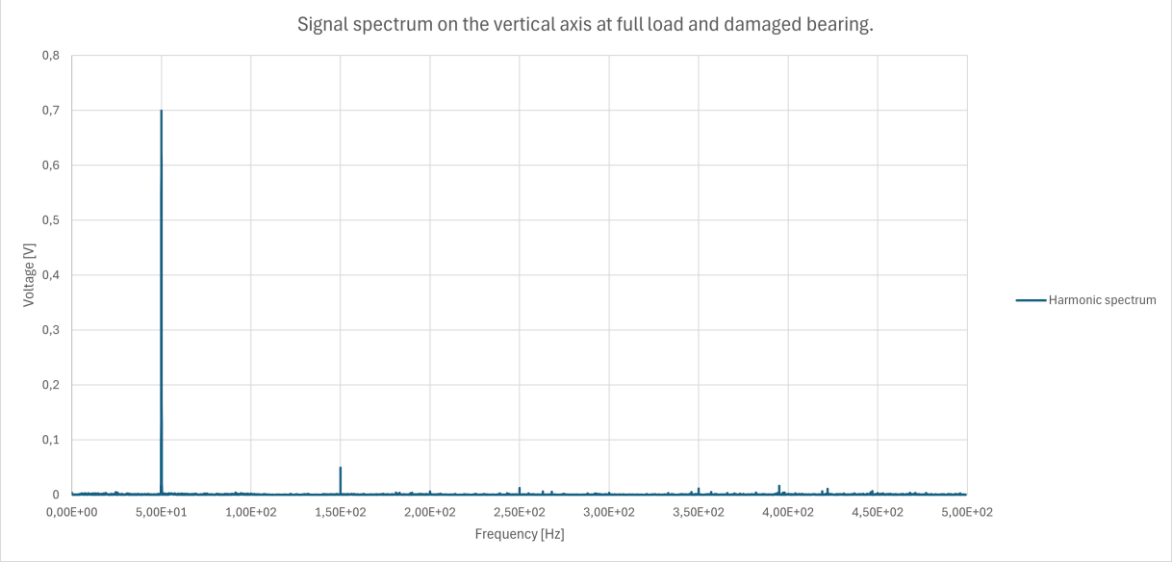

Figure 48 - Signal spectrum of the vertical axis accelerometer output, at full load condition and damaged bearing on the outer race.

Again, the results provided in Figure 49 and Figure 50 show the conditioned signal, obtained from the horizontal axis accelerometer, represented in the time and frequency domains, with the motor operating at the same rotation speed as the previous test and the same load torque.

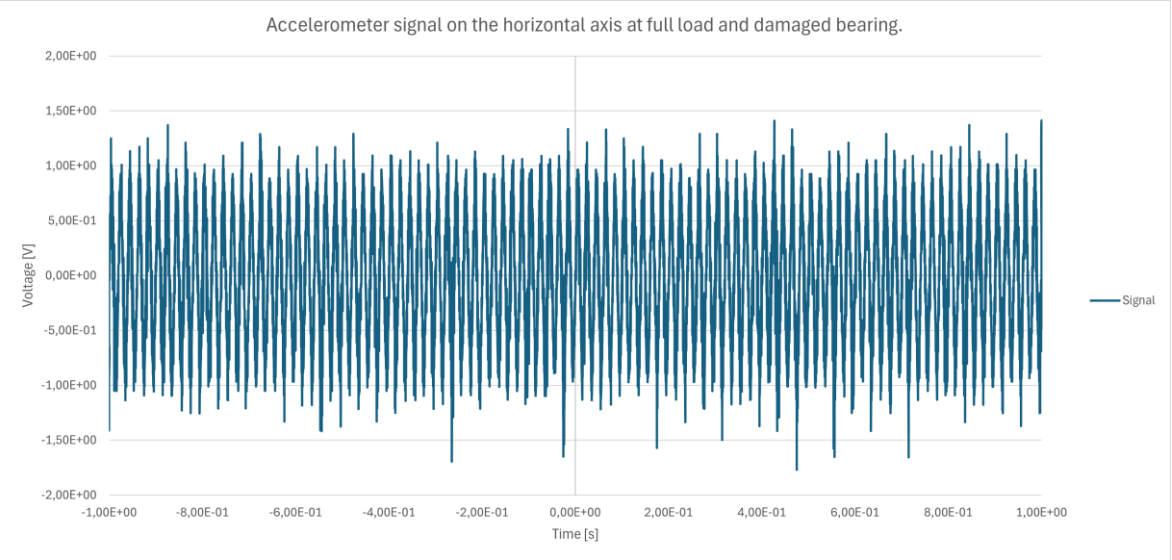

Figure 49 – Output signal of the horizontal axis accelerometer, at full load condition and damaged bearing on the outer race.

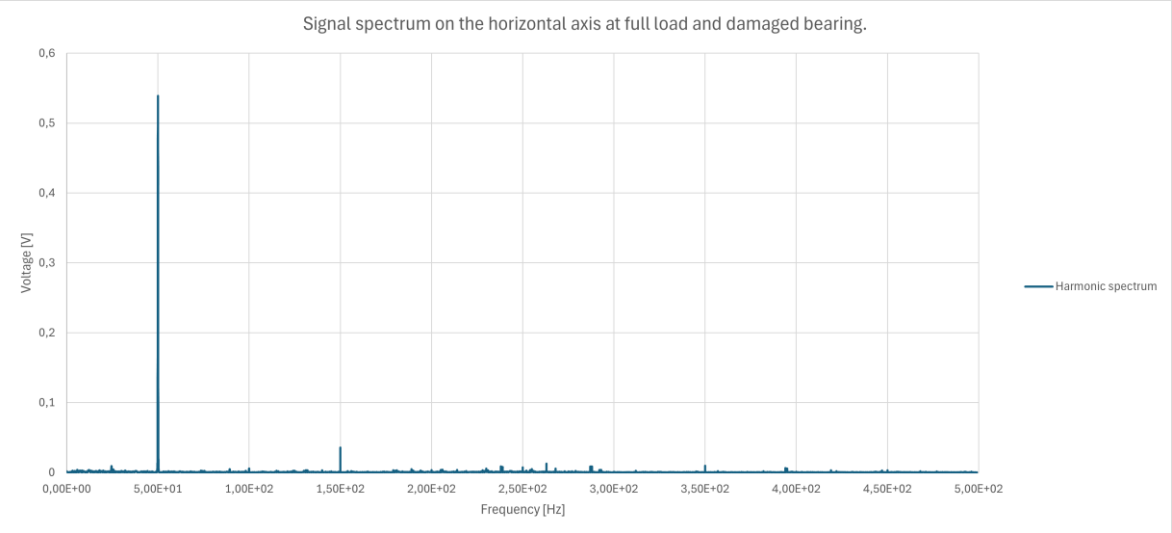

Figure 50 - Signal spectrum of the horizontal axis accelerometer output, at full load condition and damaged bearing on the outer race.

The last results, presented in Figure 51 and Figure 52, show the conditioned signal, obtained from the axial axis accelerometer, represented in the time and frequency domains, with the motor operating at the same full load regime.

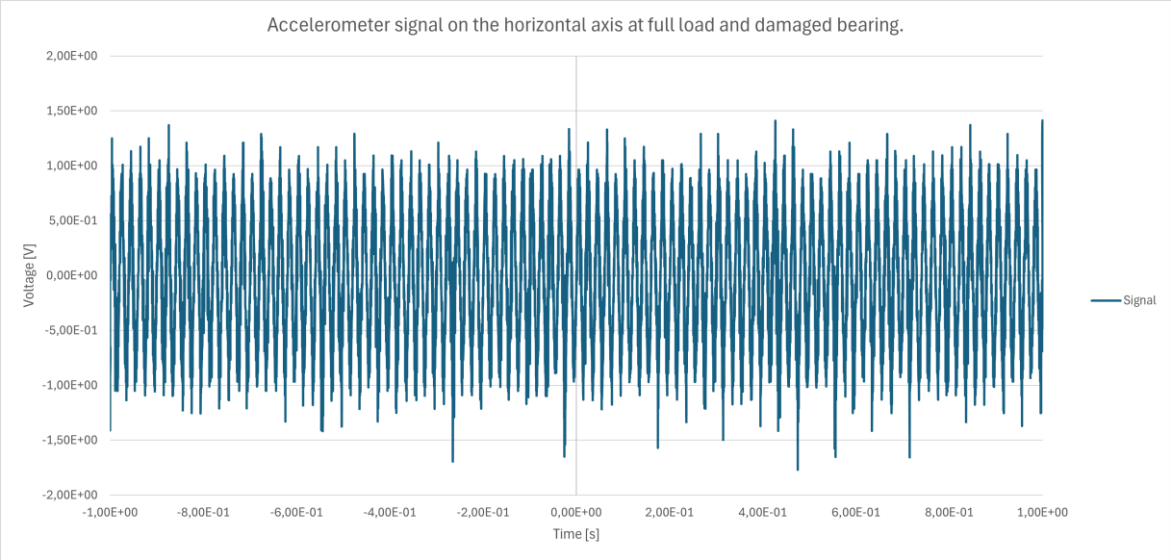

Figure 51 – Output signal of the axial axis accelerometer, at full load condition and damaged bearing on the outer race.

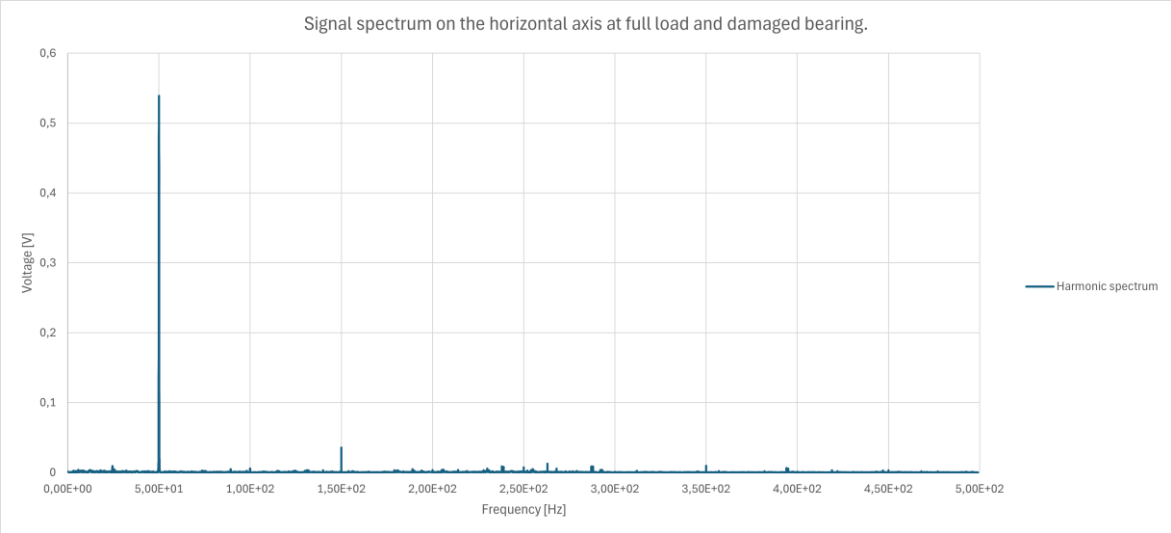

Figure 52 - Signal spectrum of the axial axis accelerometer output, at full load condition and damaged bearing on the outer race.

4.4. Analysis of results

The results of the experimental tests are analysed in more depth in this section. The damaged bearing, from SKF, model 6206-2Z, has a 2 mm hole in the outer ring of the bearing. Because of the variation of the motor rotational speed, the natural frequencies associated to the bearing components change according to the applied load torque. To diagnose damage or faults using acceleration transducers, in this case piezoelectric accelerometers, the correct placement of the sensor at the different measurement points of the motor is particularly important. The closer to the location where the bearing is located, the better the data collected will be. Therefore, the quality of information on the bearing's condition will also be improved. The accelerometer was fixed using a magnetic base. Figure 53 illustrates the points where the accelerometers were placed during the tests.

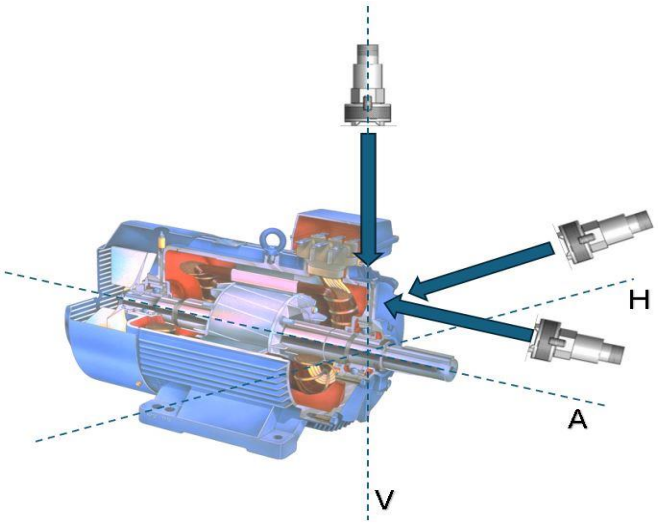

Figure 53 - Distribution of measurement points for testing vibration.

The geometric characteristics and properties of the SKF bearing used in the tests are described in Table 9 [20].

Table 9 - Dimensions, properties, and performance of the SKF 6206-2Z bearing.

Principal dimensions	***SKF 6206-2Z***
Bore (d)	30 (mm)
Outer diameter (D)	62 (mm)
Width (B)	16 (mm)
Primitive diameter (Dp)	46 (mm)
Rolling body diameter (Dcr)	12 (mm)
Number of spheres (Ncr)	9
Contact angle (β)	0 (°)

Basic load ratings	
Dynamic (C)	20.3 (kN)
Static (Co)	11.2 (kN)
Fatigue load limit (Pu)	0.475
Speed ratings	
Reference (n_ref)	24000 (r/min)
Limiting (n_lim)	12000 (r/min)

Based on equation (1), the point frequencies associated with the outer ring of the bearing, for the three load torque conditions imposed on the motor are those described in Table 10.

Table 10 - Point frequencies on the outer ring for different load torques.

Frequency	***Hertz***
f_bor (no load)	89,205
f_bor (half load)	87,599
f_bor (full load)	85,756

Using (4), the characteristic bearing frequencies were calculated in the three load torque regimes and with the coefficient "k" set up to K = 12. It is possible to verify the significant number of characteristic frequencies, which depend on the conditions under which the tests were carried out.

Table 11 - Table of characteristic frequencies in different operating regimes.

	Characteristic frequencies [Hz]		
k	f_cf (no load)	f_cf (half load)	f_cf (full load)
1	89,205	87,599	85,756
2	178,41	175,198	171,512
3	267,615	262,797	257,268
4	356,82	350,396	343,024
5	446,025	437,995	428,78
6	535,23	525,594	514,536
7	624,435	613,193	600,292
8	713,64	700,792	686,048
9	802,845	788,391	771,804
10	892,05	875,99	857,56
11	981,255	963,589	943,316
12	1070,46	1051,188	1029,072

Having obtained the characteristic frequencies, the next step is to analyse the results based on the vibration spectrograms. Figure 54 shows the vibration spectrogram corresponding to the test carried out with a healthy motor, without damage on the bearing, in the no-load scenario. All three axis are evaluated.

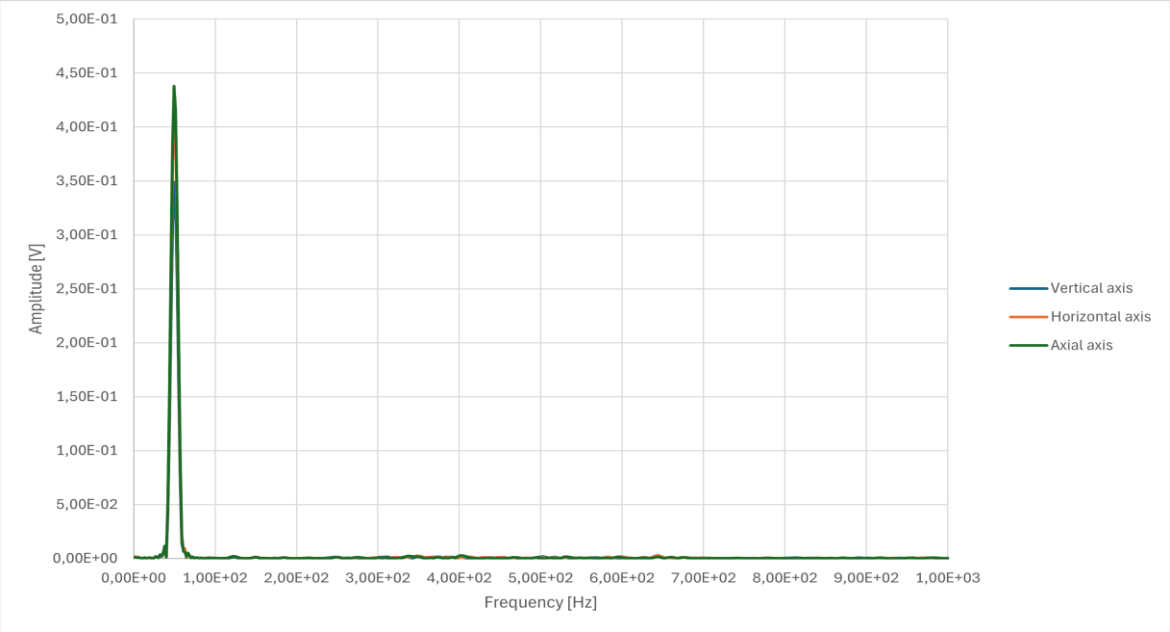

Figure 54 – Vibration spectrogram obtained for healthy motor condition, in the no-load regime, for the three measurement axes.

From Figure 54, it is possible to notice the absence of frequencies that indicate the presence of any type of anomaly or failure.

Figure 55 shows the vibration spectrogram corresponding to the test carried out with a healthy motor, in the half load torque scenario:

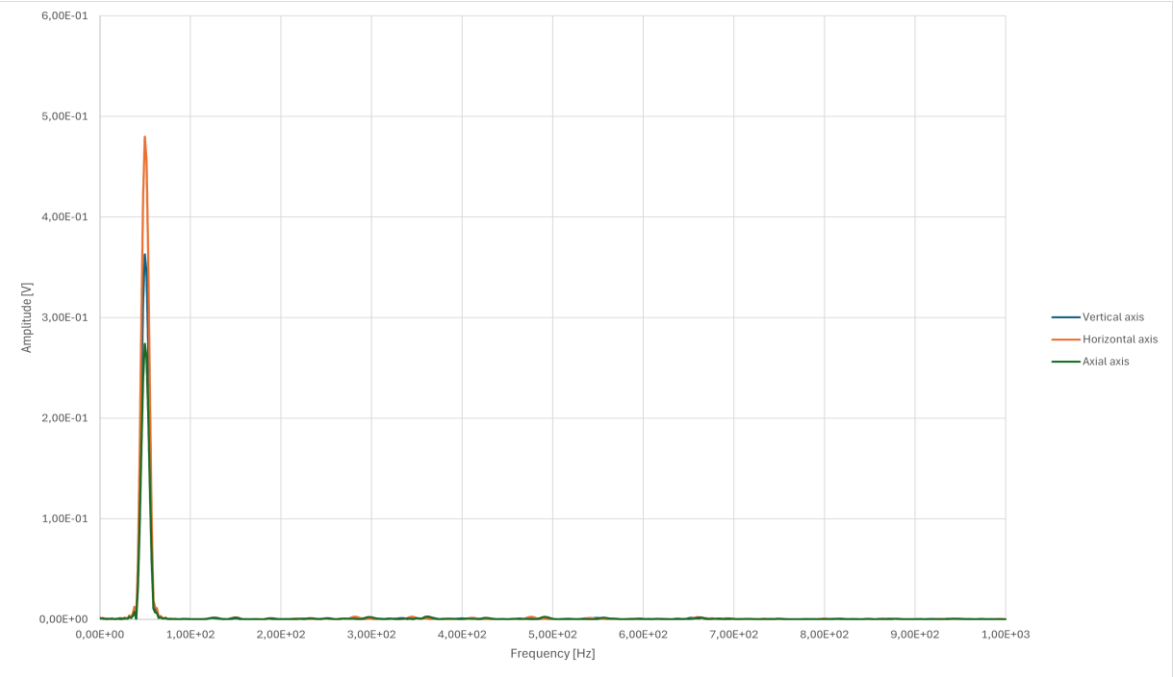

Figure 55 - Vibration spectrogram obtained for healthy motor condition, in the half load torque regime, for the three measurement axes.

It is possible to see that the amplitude of the 50 Hz harmonic decreases, when compared to the no-load regime. Such decrease is more evident in the axial and vertical axes. Moreover, the reduced amplitudes of the bearing characteristic frequencies confirm that there are no anomalies and that there are reduced levels of vibration. To conclude the analysis of results for the motor with a healthy bearing, Figure 56 presents the vibration spectrogram, in the three measurement axes, with the motor subjected to maximum load torque.

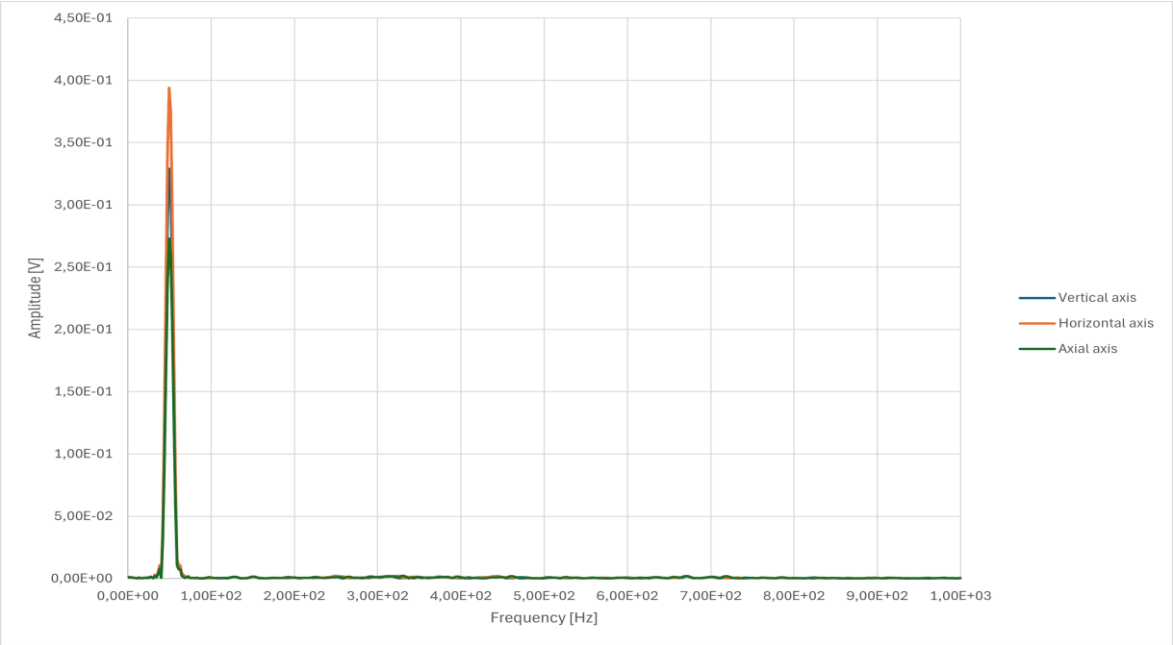

Figure 56 - Vibration spectrogram obtained for healthy motor condition, in full load torque regime, for the three measurement axes.

Again, as expected, the spectrogram is characterised by the presence of extremely low vibration levels and by the absence of frequencies that could signal the beginning, or even the presence, of some type of anomaly.

Next, the analysis focuses on the results obtained after placing a bearing with damage on the outer ring. It is expected that the spectral components in Table 11 will appear in the vibration spectrogram, in the three measurement axes, for each load regime imposed on the motor.

Firstly, Figure 57 shows the vibration spectrogram for the motor operating at no load, with the damaged bearing.

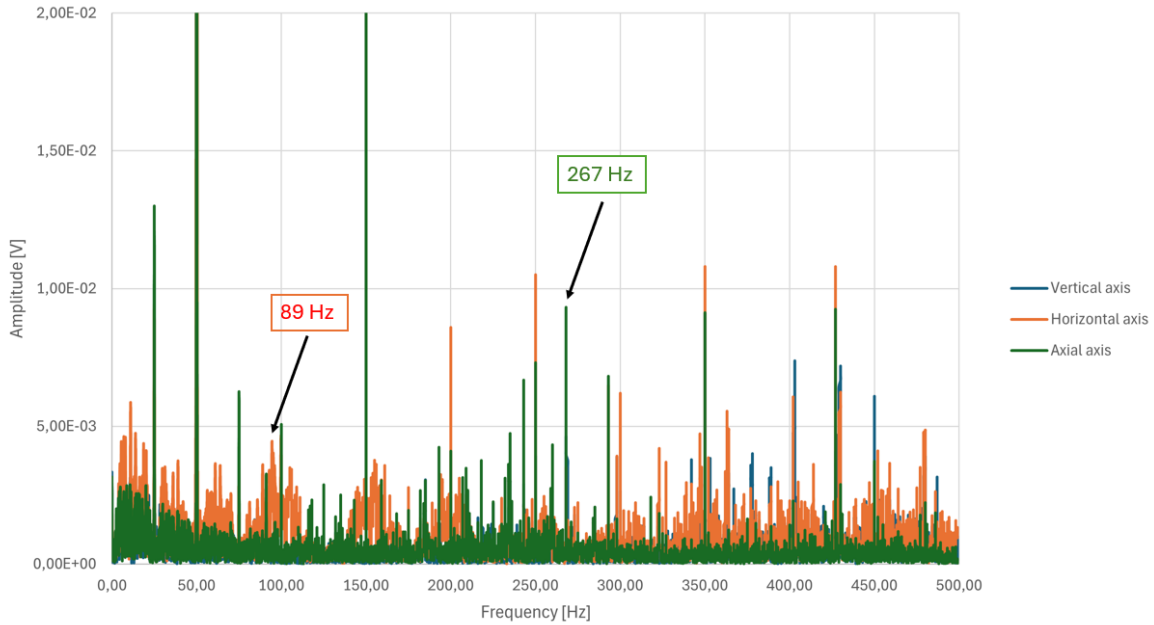

Figure 57 – Vibration spectrogram obtained for the faulty bearing, with a 2 mm hole in the outer ring, under no-load condition.

The results immediately show the appearance of spectral components associated with the frequencies identified in Table 11, as well as an increase in vibration levels, when compared to the levels obtained in the test with the undamaged bearing. The spectral components that are most evident are those measured in the axial axis.

Figure 58 shows the vibration spectrogram for the motor operating at half load torque, with the damaged bearing.

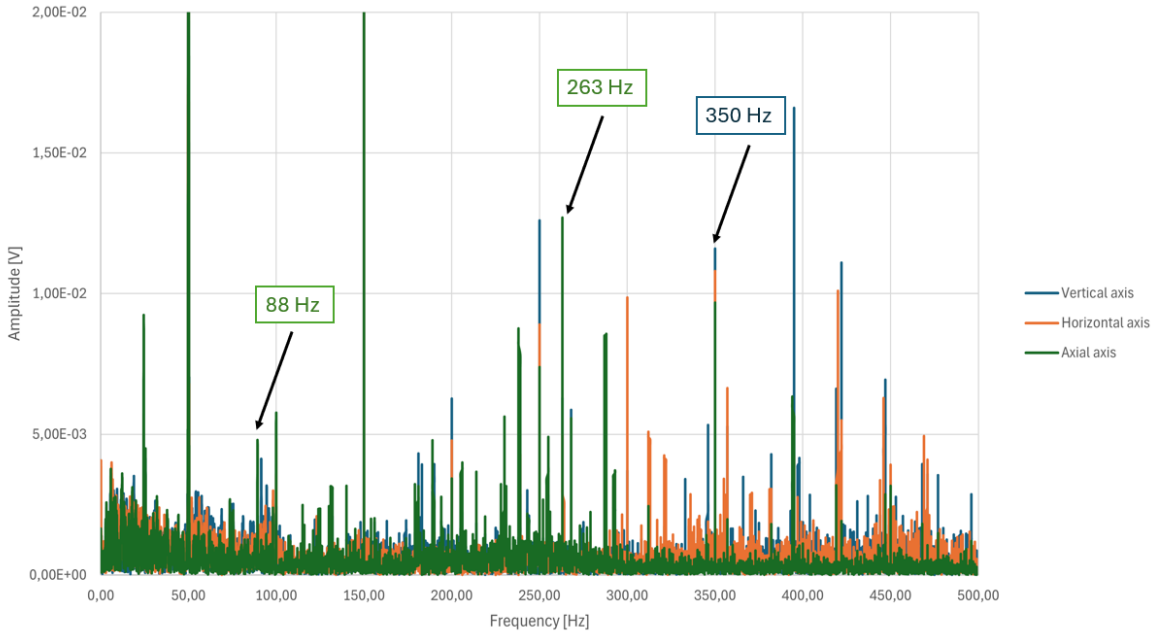

Figure 58 - Vibration spectrogram obtained for the faulty bearing, with a 2 mm hole in the outer ring, under half load torque condition.

The results presented in Figure 58 show an increase in the amplitude of multiple spectral components, compared to the test carried out with the unloaded motor. The increase in the vibration energy provides more signs of the presence of an anomaly. It is possible to observe the appearance of the fundamental frequency, at 88 Hz, as well as the frequency associated with the third and fourth harmonics.

Finally, the load torque was increased to the maximum level, with the Figure 59 showing the spectrogram resulting from the measurement of the vibrations for such condition.

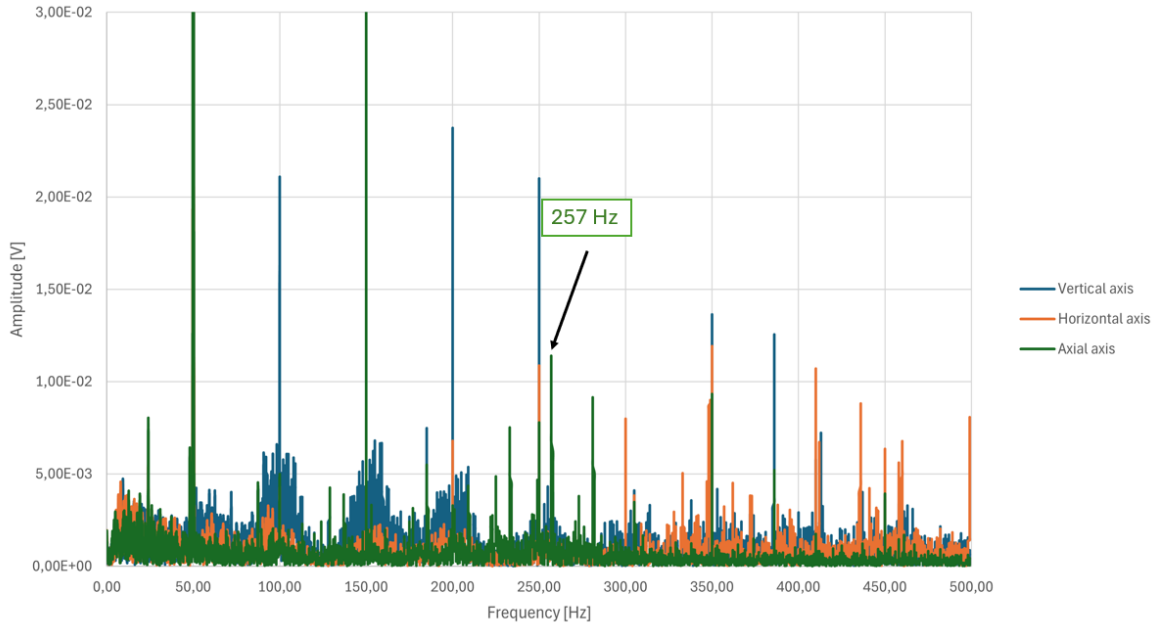

Figure 59 - Vibration spectrogram obtained for the faulty bearing, with a 2 mm hole in the outer ring, under full load torque condition.

The trend for the amplitude of the spectral components to increase continues. Increasing the load level results in the appearance of the third harmonic, like the previous results. The entire spectrum presents higher energy levels, when compared to the healthy bearing condition, in the same operating regime.

The results obtained for the frequencies predicted in Table 11, for a no-load regime, are presented in Table 12, allowing comparison of the amplitudes of the relevant harmonics.

Table 12 - Amplitudes for no-load condition.

Characteristic frequencies [Hz]	***Amplitudes [V]***					
	Healthy			**Faulty**		
	Vertical	Horizontal	Axial	Vertical	Horizontal	Axial
89,205	0,0005	0,0008	0,0003	0,001	0,004	0,0008
178,41	0,0005	0,0003	0,0001	0,0004	0,0006	0,0006
267,615	0,0006	0,0004	0,0002	0,005	0,003	0,009
356,82	0,0003	0,0001	0,0007	0,002	0,002	0,0005
446,025	0,0004	0,0009	0,0004	0,002	0,002	0,0008

The results obtained for the frequencies predicted in Table 11, for a half-load regime, are presented in Table 13, allowing, again, to compare the amplitudes of the relevant harmonics.

Table 13 - Amplitudes for half-load condition.

Characteristic frequencies [Hz]	***Amplitudes [V]***					
	Healthy			**Faulty**		
	Vertical	Horizontal	Axial	Vertical	Horizontal	Axial
87,599	0,0003	0,0004	0,0003	0,0008	0,0008	0,005
175,198	0,0002	0,0002	0,0001	0,0006	0,0005	0,0006
262,797	0,0008	0,0007	0,0007	0,006	0,005	0,012
350,396	0,0001	0,0009	0,0002	0,012	0,010	0,009
437,995	0,0002	0,0003	0,0004	0,003	0,001	0,0003

Finally, the results obtained for a maximum load regime are presented in Table 14, allowing the amplitudes of the relevant harmonics to be compared.

Table 14 - Amplitudes for full-load condition.

Characteristic frequencies [Hz]	***Amplitudes [V]***					
	Healthy			**Faulty**		
	Vertical	Horizontal	Axial	Vertical	Horizontal	Axial
87,599	0,0003	0,0002	0,0001	0,001	0,001	0,0008
175,198	0,0004	0,0005	0,0006	0,002	0,001	0,001
262,797	0,0004	0,0007	0,0001	0,004	0,002	0,011
350,396	0,0005	0,0007	0,0008	0,002	0,002	0,0003
437,995	0,0002	0,0002	0,0001	0,001	0,001	0,0002

Chapter 5

Conclusions

5.1. General considerations

The work presented in this dissertation refers to the idealisation, sizing, and implementation of a data acquisition system, embedded in the housing of an electric motor, capable of assisting in the diagnosis and analysis of faults and breakdowns in a three-phase induction motor. Furthermore, it allows to export data to a computer connected to the Internet, to obtain a database on the operating status of the equipment.

As described in Chapter 1, the importance of evaluating the operating status of this type of equipment is of great importance, so the implementation of a device capable of continuously monitoring the motor's performance justifies further investigation and more detailed study, to minimize the costs associated with periodic inspections. Knowing that at least half of all induction motor failures are related to bearings, it was natural to choose the bearing failure to serve as a reference for the designed prototype.

By using the laboratory setup adjusted to the type of damage in question, with access to equipment capable of simulating different types of load torques and performing fast Fourier analysis of the signal, the conditions were met to carry out various tests on the signal acquisition system, making it possible to experimentally observe the designed cut-off frequency, the offset required for the accelerometer signal, in order to remain in line with the voltage admitted by the microcontroller's ADC and the adjustable gain, which provides flexibility for the integration of accelerometers with different levels of sensitivity.

In this study, it is concluded that the design projects for an analogue data acquisition system, namely acceleration transducers, require the correct dimensioning of the signal conditioning circuits, with computer simulation not being enough for this, as well as physical tests in test board, before moving on to the production of the printed circuit board. It should be noted that the piezoelectric accelerometer used has the disadvantage of not being externally powered, nor having an internal signal conditioning circuit, meaning that the design of the data acquisition system becomes more complex. The cables connecting the sensor to the board must guarantee a good connection and high noise immunity.

In the specific case of carrying out the design of electrical circuits using computer-aided design software, attention must be paid to the recommendations of the component manufacturers, expressed in their datasheets, to ensure that the specifications are in

accordance with the components capabilities and that the components are properly sized in terms of rated voltages and currents. Also, it is relevant to follow the manufacturer's recommendations for the placement of passive components, as well as the layout recommendations on the circuit board, to reduce possible interference or increase impedances. It is important to pay attention to the width of the wires, depending on the current that will flow through them. During the board design phase, it is relevant to make sure that the design requirements are in line with the manufacturer's production capabilities.

A practical limitation of the model presented in this study has to do with the quality of the accelerometers used in the experimental tests. The results obtained would have been of enhanced quality if new, better-quality accelerometers had been used.

Finally, it is concluded that the practical results of the tests carried out were aligned with the theoretical principles. The 2 mm hole in the bearing outer ring introduces low amplitude vibrations in the spectrogram. With careful analysis and comparison with the data produced with a healthy motor, it is possible to identify the fault at an early stage of development. The diagnosis of mechanical defects in the three-phase induction motor allows determining the presence of a fault, its location, and its degrees of severity.

5.2. Suggestions for future work

Having finished the presentation of the dissertation work developed within the scope of the design, validation, and implementation of a condition monitoring device for three-phase induction motors, it is important to mention some aspects and suggestions that can be improved and developed in the future, related to the subject addressed in this work.

It is important to extend the study of the signal conditioning circuit to other types of faults, such as poor lubrication or broken rotor bars. The study was only focused on the concept of developing the data acquisition board, and it would be interesting, in the future, to implement software on the microcontroller, which makes use of a library created to compute, in real time, the FFT on the ESP32 and obtain the frequency and amplitude of the signal, and export the data directly via Wi-Fi to a computer, which allows to view the collected data in a personalized graphical environment depending on the power of the equipment being monitored.

It would also be interesting to design a housing built using 3D printing for the PCB, with a coupling system to the motor housing and allowing the alert LEDs to be displayed on site.

Finally, future work is proposed to detect any failures or malfunctions in loads coupled to the three-phase induction motor, such as fans or gearboxes.

Bibliographic references

[1] A. J. Marques Cardoso, S. M. A. Cruz, D. S. B. Fonseca, "Inter-turn stator winding fault diagnosis in three-phase induction motors, by Park's vector approach", *IEEE Transactions on Energy Conversion*, vol. 14, pp. 595-598, 1999.

[2] Informain – Maintenance Institute Information Technologies, S.A., Serviços de Engenharia de Manutenção, "Conceitos de medições de vibrações", 2023.

[3] Antonio J. Marques Cardoso, *Diagnóstico de Avarias Em Motores de Indução Trifásicos*. Coimbra Editora, Coimbra, 1991.

[4] V. L. L. Costa, B. Eberhardt, J. Chen and J. Roßmann, "Towards Predictive Maintenance: an Edge-based Vibration Monitoring System in Industry 4.0," *2023 International Conference on Sustainable Computing and Data Communication Systems (ICSCDS)*, Erode, India, 2023

[5] M. Blodt, P. Granjon, B. Raison and G. Rostaing, "Models for Bearing Damage Detection in Induction Motors Using Stator Current Monitoring," in *IEEE Transactions on Industrial Electronics*, vol. 55, no. 4, pp. 1813-1822, April 2008

[6] J. L. H. Silva, "Diagnóstico e análise de avarias nos rolamentos de motores de indução trifásicos", 2005. Accessed: 17 March 2024. [Online]. Available: https://estudogeral.uc.pt/handle/10316/13956

[7] B. Li, M. Chow, Y. Tipsuwan, J. C. Hung, "Neural-network-based motor rolling bearing fault diagnosis", *IEEE Transactions on Industrial Electronics*, vol. 47, no. 5, pp. 1060-1069, Oct. 2000.

[8] Georges Asch, "Acquisition de données; du capteur à l'ordinateur (3e édition)", Dunod, Technique Et Ingeniere, 06/04/2011.

[9] ISO 20816-1:2016 "Mechanical Vibration – Measurement and evaluation of machine vibration – Part 1 – General Guidelines.

[10] Brüel & Kjær, Measuring Vibration the Complete Guide. Accessed: 17 March 2024. [Online]. Available: https://www.bksv.com/pt/knowledge/blog/vibration/measuring-vibration

[11] E. M. Stein, and Guido Weiss. "*Introduction to Fourier Analysis on Euclidean Spaces (PMS-32)*". Princeton University Press, 1971. Accessed: 17 March 2024. [Online]. Available: https://books.google.pt/books?id=YUCV678MNAIC&lpg=PP15&ots=KQD3DeSXMz&dq=introduction%20to%20fourier%20analysis%20on%20euclidean%20spaces&lr&hl=pt-

BR&pg=PP7#v=onepage&q=introduction%20to%20fourier%20analysis%20on%20euclidean%20spaces&f=false

[12] Emerson, Machinery Health Accelerometers. Accessed: 17 March 2024. [Online]. Available: https://www.emerson.com/documents/automation/specifications-sheet-industrial-accelerometer-a0760gp-ams-en-39590.pdf

[13] IEC 60529, International Electrotechnical Commission. Accessed: 17 March 2024. [Online]. Available: https://www.wewontech.com/IEC60529-%20IP-Standard.pdf

[14] IEC 60068-2-27, International Electrotechnical Commission. Accessed: 17 March 2024. [Online]. Available: https://webstore.iec.ch/publication/12709&preview=1

[15] IEC 60068-2-64, International Electrotechnical Commission. Accessed: 17 March 2024. [Online]. Available: https://webstore.iec.ch/publication/65892

[16] IEC 60079, International Electrotechnical Commission. Accessed: 17 March 2024. [Online]. Available: https://webstore.iec.ch/publication/62417

[17] Espressif Systems: Wireless SOCs, Software, Cloud and AIoT, ESP32-DevKitC V4 Getting Started Guide. Accessed: 17 March 2024. [Online]. Available: https://docs.espressif.com/projects/esp-idf/en/stable/esp32/hw-reference/esp32/get-started-devkitc.html#get-started-esp32-devkitc-board-front

[18] D. Ashlock, A. Warren, "The Engineer´s Guide to Signal Conditioning", National Instruments, 2015. Accessed: 17 March 2024 [Online]. Available: https://download.ni.com/evaluation/signal_conditioning/20712_Benefits_of_Integrated_SC_WP_HL.pdf

[19] B. Carter, "Designing Gain and Offset in Thirty Seconds", Texas Instruments, Application report, February 2022. Accessed: 17 March 2024 [Online] Available: https://www.ti.com/lit/an/sloa097/sloa097.pdf?ts=1724346156419

[20] SKF Group, 6206-2Z Deep groove ball bearing with seals or shields. Accessed: 17 March 2024. [Online]. Available: https://www.skf.com/my/products/rolling-bearings/ball-bearings/deep-groove-ball-bearings/productid-6206-2Z

Appendix

PCB Design

After validation in computer simulation and in the experimental tests, the design of the signal acquisition system was implemented in printed circuit board design software. The software used is free to use, made available by the Chinese manufacturer JLCPCB and called EasyEDA. It is an intuitive environment, with access to a vast component library, which already includes the component footprint, as well as a link to the manufacturer's datasheet. As the components are implemented in the schematic, it is possible to choose, for the same types of components, the prices and availability of the supplier. These parameters are important when ordering the plates. As it is a software provided by the manufacturer, it is possible to consult the manufacturing and assembly capabilities of the PCB, to satisfy the PCB specifications with different production capacities.

The schematic of the signal acquisition system design, coming from three piezoelectric accelerometers, powered by a 15 V voltage source, is represented in Figure 60 and Figure 61.

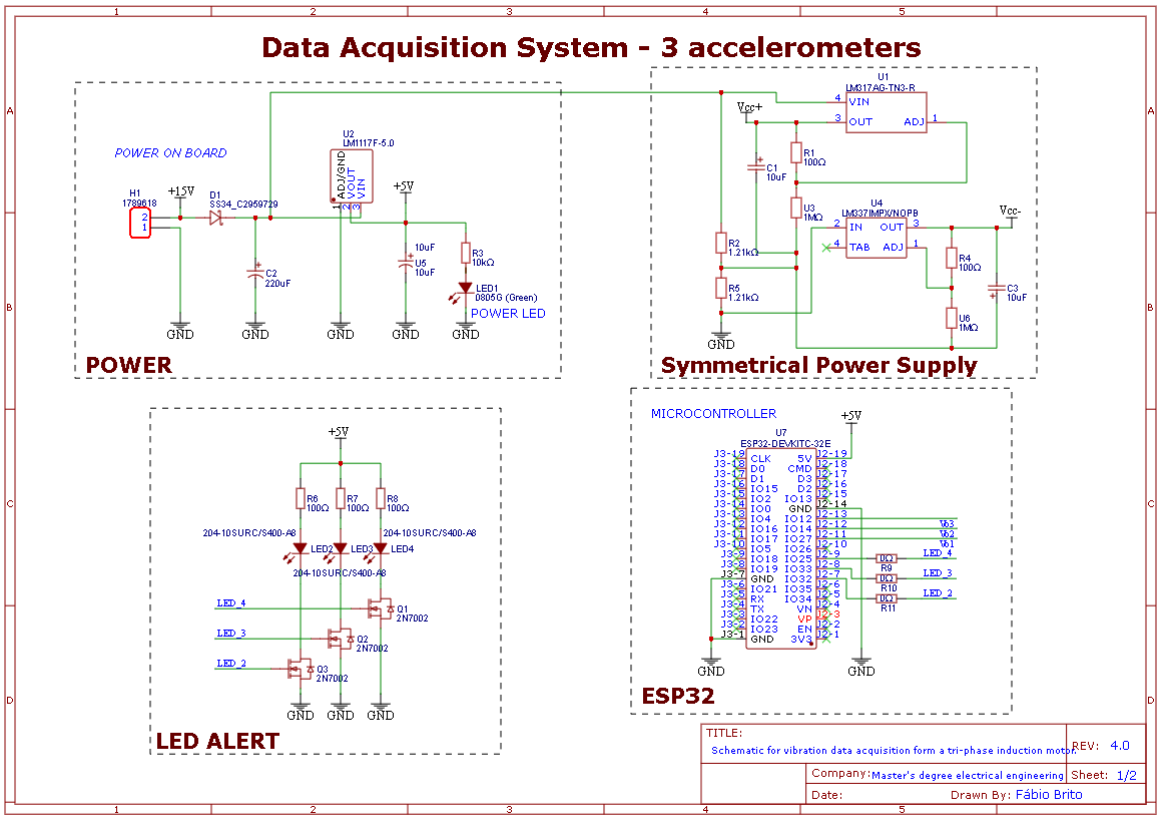

Figure 60 - Sheet 1 of the electronic circuit schematic.

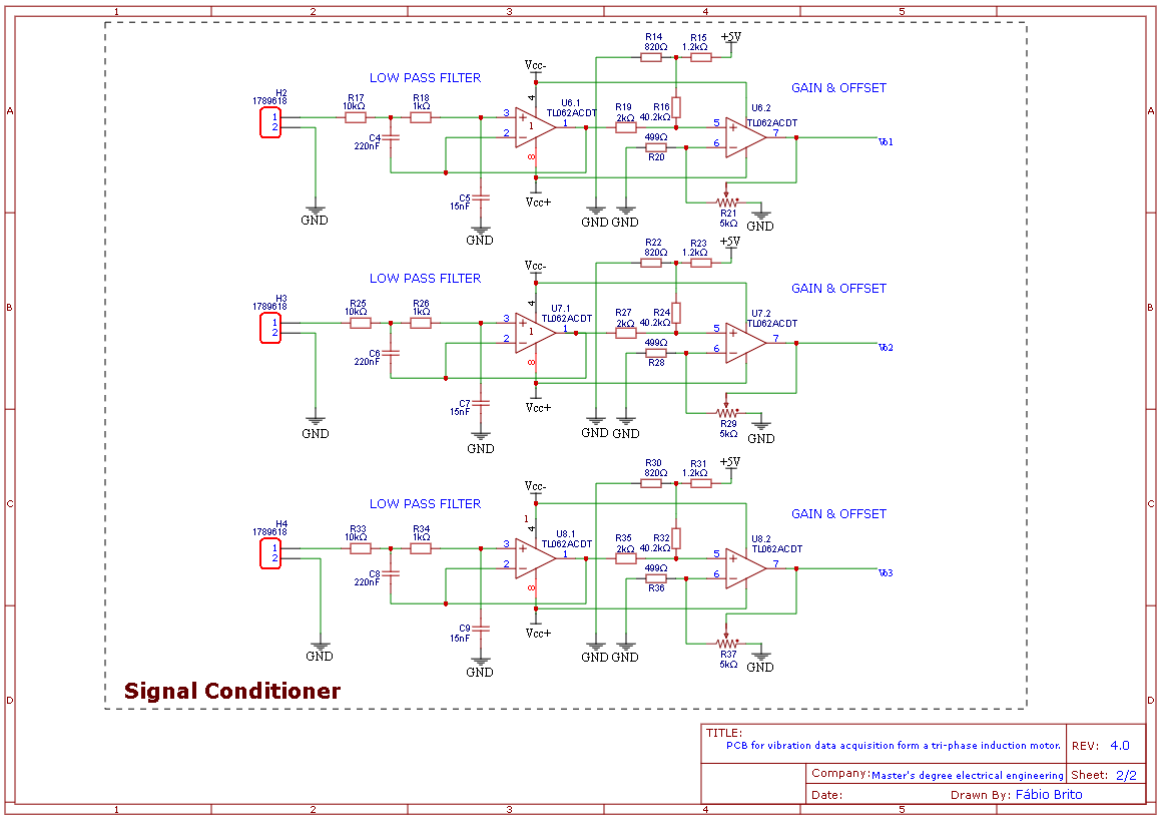

Figure 61 - Sheet 2 of the electronic circuit schematic.

Figure 60 and Figure 61 represent the various modules that make up the printed circuit board (PCB). Each module is surrounded by a dashed square. In Figure 60, the first module concerns the system power supply. An LM1117F voltage regulator reduces the input voltage to 5 V, which will power the alert system based on LEDs, power the ESP32 microcontroller and the offset circuit. On the same sheet, there is also the symmetrical power supply module, which makes use of two voltage regulators, the LM317AG with +7 V output to power the positive input of the OPAMP, and the LM337IMPX/NOPB with -7V output to feed the negative input of the OPAMP. The second sheet, in Figure 61, contains the circuit responsible for acquiring the signal, filtering, amplifying, and offsetting. In the schematic, the different signal conditioning stages are duly identified. The PCB design consists of four layers, three of which are for signal and an internal layer for ground. The design starting point is the definition of the board's contour measurements. The plate has dimensions of 82 mm by 88 mm. Four holes were placed in each corner with a 3 mm diameter, to allow the plate to be embedded inside a protective casing.

Figure 62 to Figure 65 illustrate the different layers that make up the printed circuit board.

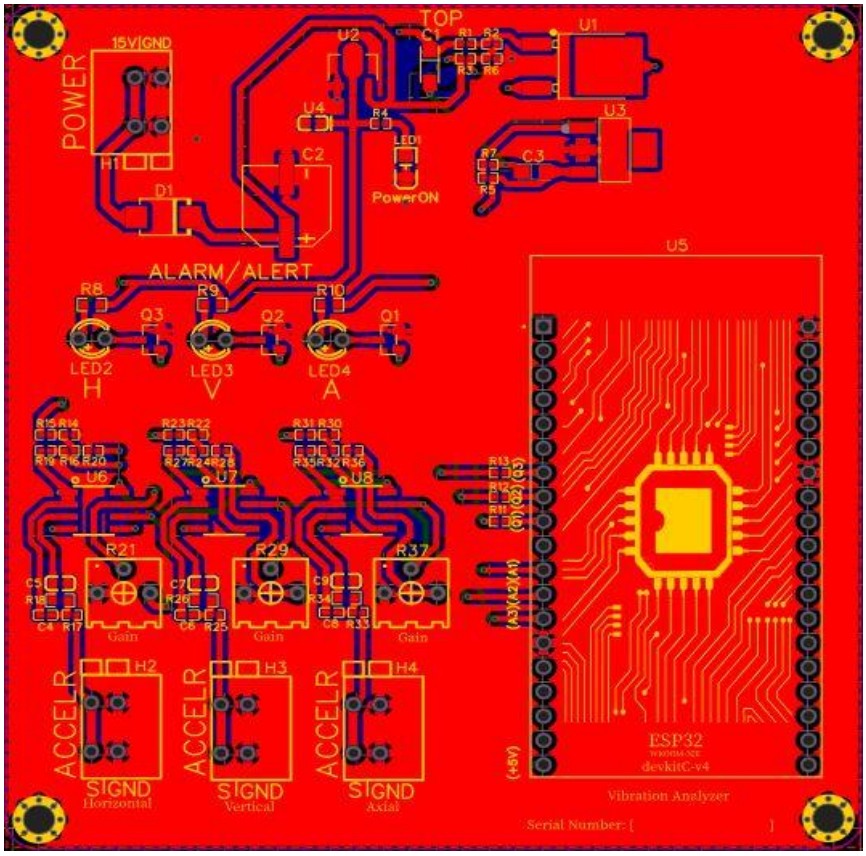

Figure 62 - Top layer.

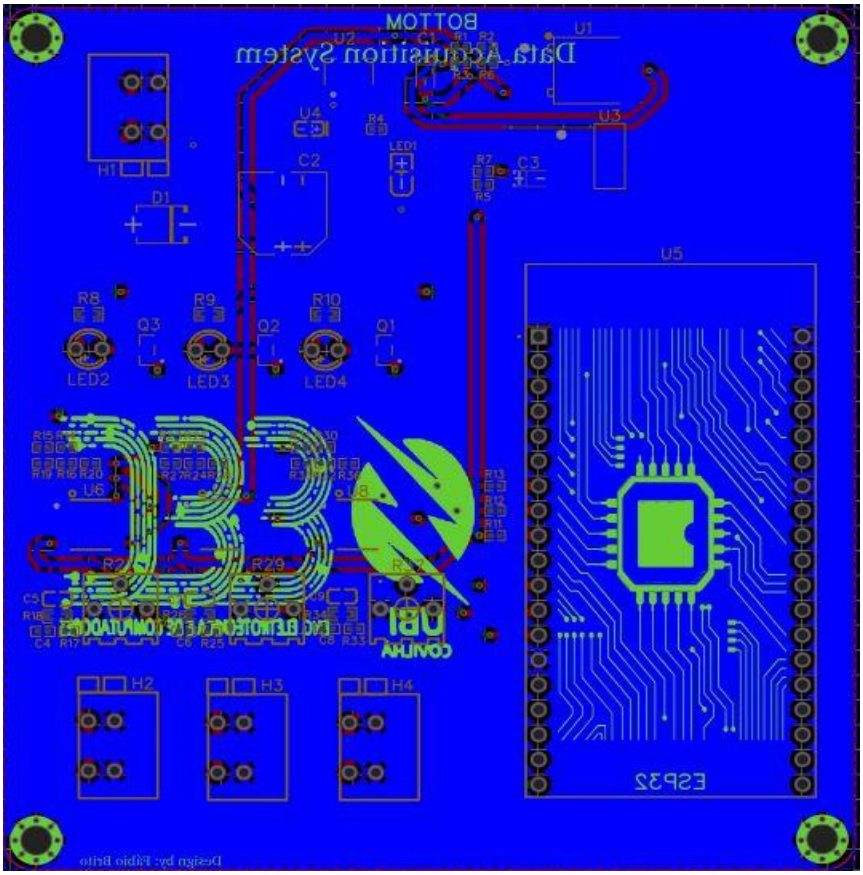

Figure 63 - Bottom layer.

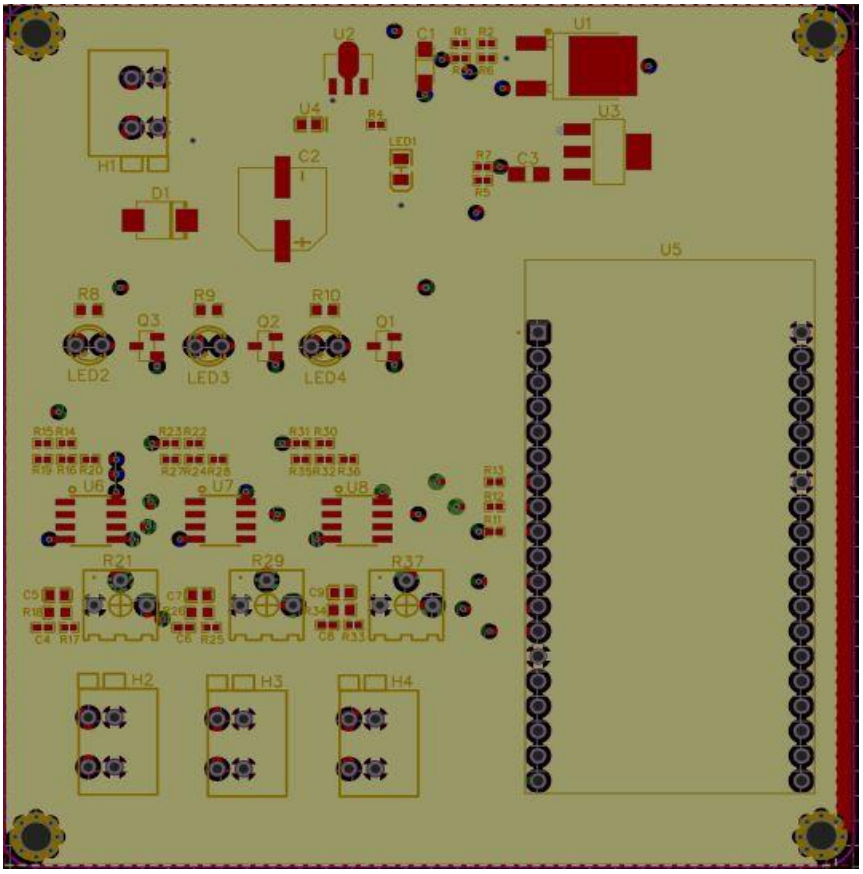

Figure 64 - Inner 1 layer.

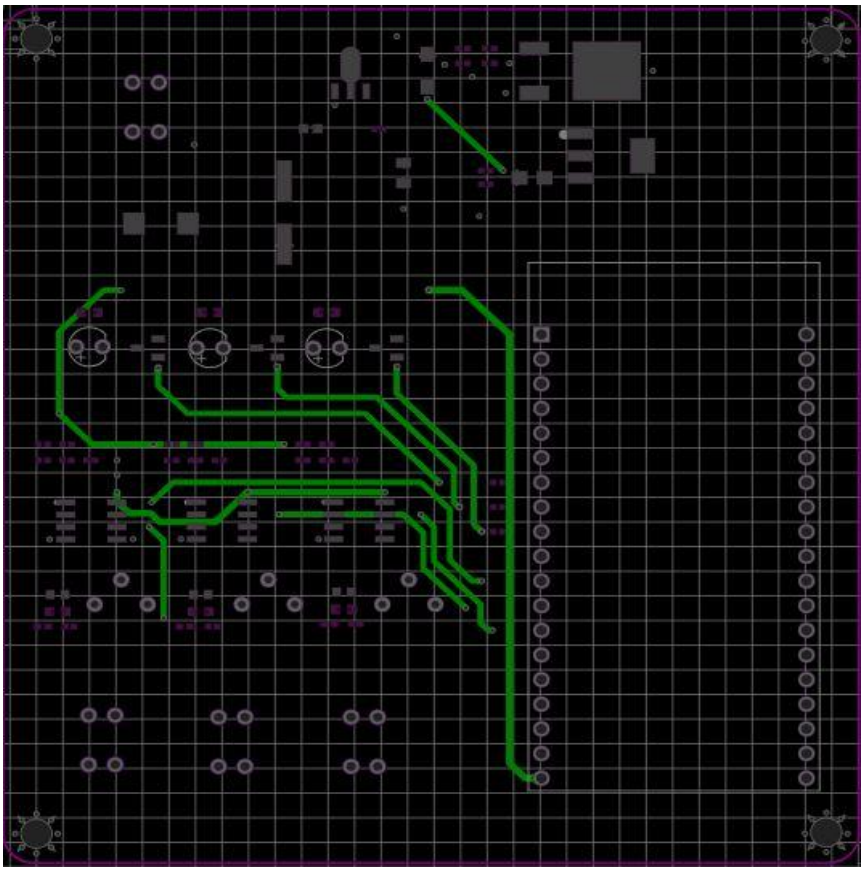

Figure 65 - Inner 2 layer.

The arrangement of the different components aims to segment the different stages, with the circuits relating to the system power supply being located in the upper left corner; the alarm and alert LEDs are located in the centre; and underneath is the offset circuit. In the slightly lower part, there are the operational amplifiers. Each signal conditioning circuit has an OPAMP for the filter and gain, since the OPAMP TL062ACDT have two OPAMPs in the same encapsulation, thus allowing them to take up less space with more components. In the lower part of the top layer of the board, you will find the headers to connect the accelerometers. The right side of the PCB receives the ESP32 development board, with the USB input facing downwards, to simplify the connection to load the software on the microcontroller. The Wi-Fi antenna is facing upwards.